EAS Synchrotron X-ray Emissions: Numerical Simulations

R. A. Torres Saavedra

Gran Sasso Science Institute

INFN-Laboratori Nazionali del Gran Sasso

: rodrigo.torressaavedra@gssi.it

37th JEM-EUSO Collaboration Meeting

Paris, France, June 2-6, 2025

Outline

The **objective**:

- compute the X-ray emissions from an EAS given a candidate primary energy and trajectory through the atmosphere.

The **procedure**:

- Adapt the emission formula from a single particle to an ensemble of particles
- Integrate over the distribution of energies
- Integrate over the trajectory under some simplifying assumptions.
- Obtain spectra of photons arriving on an ideal detection plane.

Outline: The Master Formula

$$\frac{dN_\gamma^{(EAS)}}{d\epsilon} = \int_{X_{min}}^{X_{max}} \frac{dX}{\rho(X)\,c}\, Tr(\epsilon, \Delta X)\, N(X) \int_{E_{min}}^{E_{max}} dE\, \frac{dn_e}{dE}(E, s(X))\, \frac{dN_\gamma^{(1)}}{d\epsilon}(E, \epsilon)$$

Starting from the retarded potentials for a single gyrating particle and the Poynting vector, one can derive an expression for the energy emitted per unit time and solid angle. Extending this to an ensemble of particles in the incoherent radiation regime, the expected number of photons emitted by an EAS is given by:

- the convolution of the single-particle spectrum with the electron energy distribution,
- integrated over the entire shower development.

Single particle emission

$$\frac{dN_\gamma^{(EAS)}}{d\epsilon} = \int_{X_{min}}^{X_{max}} \frac{dX}{\rho(X)\,c}\, Tr(\epsilon, \Delta X)\, N(X) \int_{E_{min}}^{E_{max}} dE\, \frac{dn_e}{dE}(E, s(X)) \boxed{\frac{dN_\gamma^{(1)}}{d\epsilon}(E, \epsilon)}$$

Single Particle Emission

- The power spectrum is proportional to the synchrotron function, **F(x)**, which depends only on, **x**, the ratio between the photon freq., **ω**, and the critical freq., $\boldsymbol{\omega_c}$.
- $\boldsymbol{\omega_c}$ depends linearly on the Larmor frequency, $\boldsymbol{\omega_L}$, which is itself linearly proportional to the magnetic field, **B**.
- The **number of photons** emitted per unit time and frequency is just the **power spectrum divided by the photon energy**.

$$\frac{P^{(1)}}{d\epsilon}(E) = \frac{\sqrt{3}\alpha}{2\pi}\omega_L F\left(x(E)\right)$$

$$\frac{dN_\gamma^{(1)}}{dtd\epsilon}(E) = \frac{\sqrt{3}\alpha}{2\pi}\frac{\omega_L}{\epsilon}F\left(x(E)\right)$$

with:

$$\omega_L = \frac{q_e||\vec{B}||}{m_e c} \qquad \omega_c = \frac{3}{2}\gamma^2\omega_L \sin\alpha_p$$

Single Particle Emission: Power Spectrum

$$F(x) = x\int_x^\infty K_{5/3}(\xi)d\xi$$

- The power spectrum, F(x), is given by the integral of a Bessel function.

For performance, two approaches were tested:

- pre-computing and evaluating it with an interpolator (right).
- an analytic approximation formula by Fouka and Ouichaoui (2013).

The latter was chosen for performance.

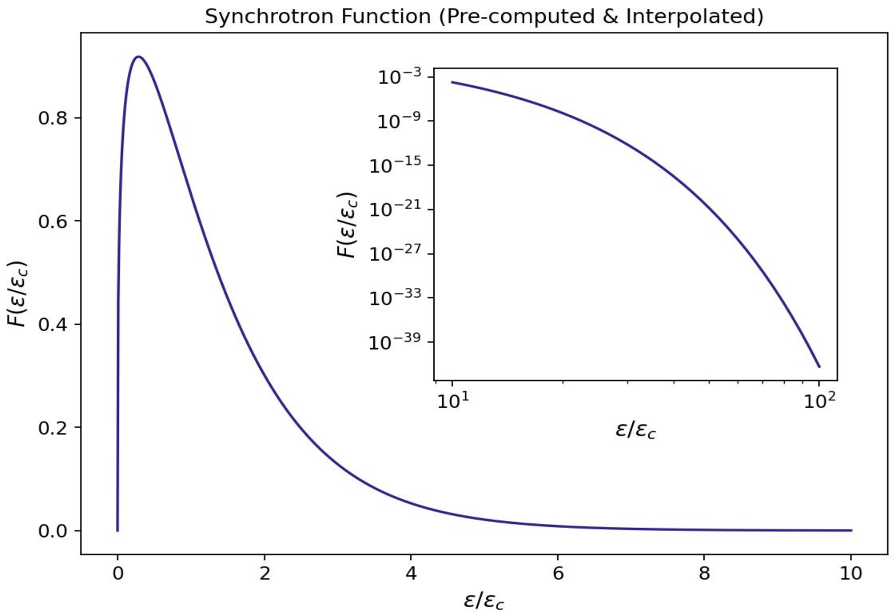

Single Particle Emission: Power Spectrum (cont.)

- Most of the power is emitted at frequencies, **ω**, close to the critical synchrotron frequency, **ω_c**
- For **ω** < **ω_c**, the power grows as a power law up to the critical frequency
- For **ω** > **ω_c**, the power falls off as an exponential (approximately)
- Larger photon frequencies require larger electron energies.

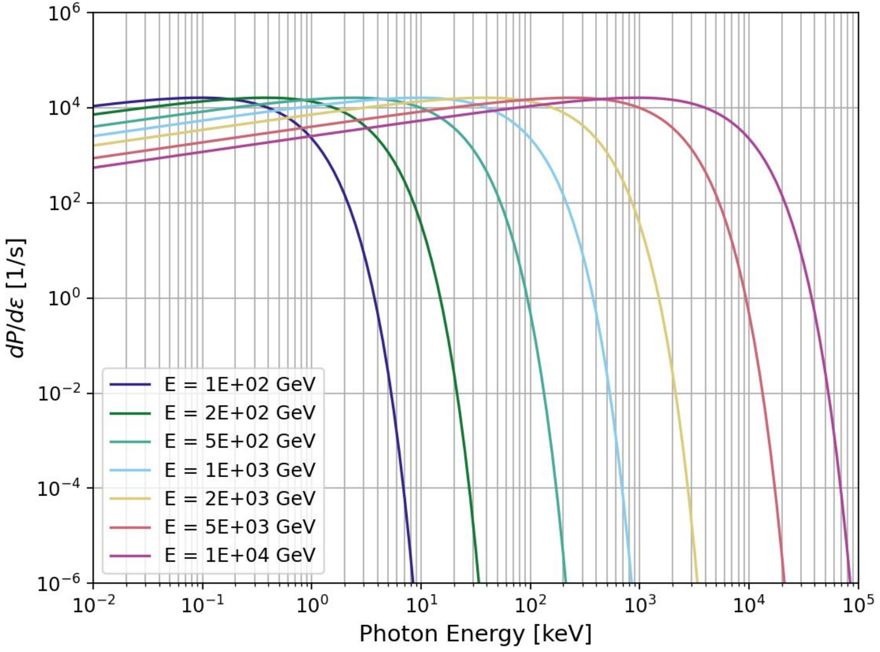

Energy Integration Limits

$$\frac{dN_\gamma^{(EAS)}}{d\epsilon} = \int_{X_{min}}^{X_{max}} \frac{dX}{\rho(X)\,c}\, Tr(\epsilon, \Delta X)\, N(X) \boxed{\int_{E_{min}}^{E_{max}} dE} \frac{dn_e}{dE}(E, s(X))\, \frac{dN_\gamma^{(1)}}{d\epsilon}(E, \epsilon)$$

Energy Integration Limits

- For a given photon energy band, one may integrate the single particle spectrum to get the number of photons emitted in that band.
- Scanning over electron energies one can obtain the range of electron energies that contribute significantly to the emissions in that band.
- The **integration limits** were chosen as going from **100 GeV** to **1 PeV** (since there are few e^- with E > 1 PeV in a shower with 100 PeV primary energy)

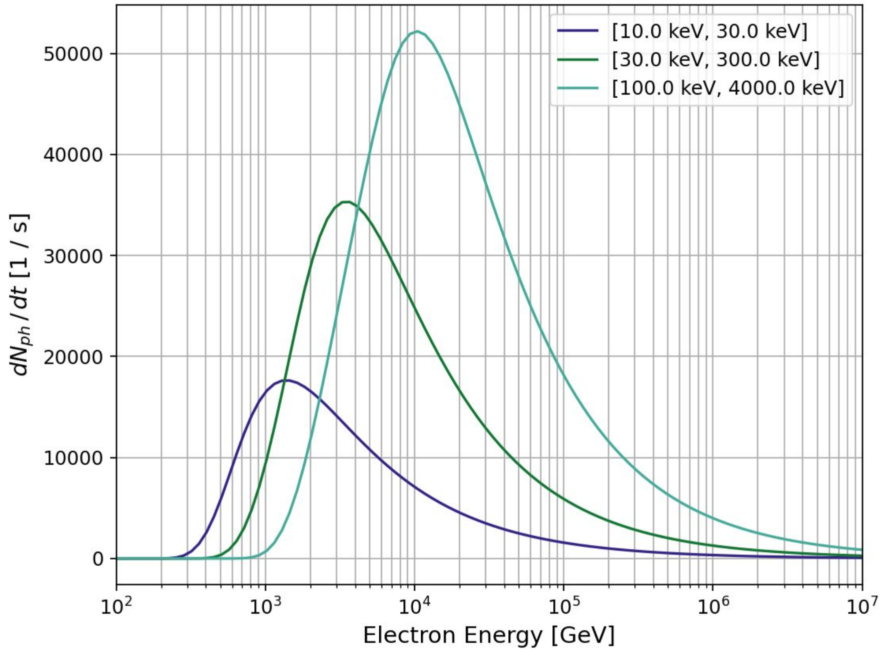

9

Electron Energy Distribution

$$\frac{dN_\gamma^{(EAS)}}{d\epsilon} = \int_{X_{min}}^{X_{max}} \frac{dX}{\rho(X)\,c}\, Tr(\epsilon, \Delta X)\, N(X) \int_{E_{min}}^{E_{max}} dE \boxed{\frac{dn_e}{dE}(E, s(X))} \frac{dN_\gamma^{(1)}}{d\epsilon}(E, \epsilon)$$

Electron Energy Distribution: Hillas

$$T(E) = \int_E^\infty dE \frac{dn_e}{dE} = \left(\frac{0.89E_* - 1.2}{E_* + E_k}\right)^s \left(1 + 10^{-4} s E_k\right)^{-2}$$

$$E_* = \begin{cases} 44 - 17(s - 1.46)^2 & s \geq 0.4 \\ 26 & \text{otherwise} \end{cases}$$

Older model (1982)

- Is an empirical fit to data obtained through MC simulations (not with CORSIKA) in bins of shower age down to s = 0.1

Limitations:

- Only photon primary showers were simulated with energies up to 1 TeV.

Electron Energy Distribution: Nerling

Newer Model (2006)

- Is in better agreement with CORSIKA simulations data near the shower maximum ($0.8 \leq s \leq 1.2$) .

Limitations:

- Has not been validated for young showers ($s < 0.8$).
- Parameterized normalization deviates slightly from unity ($s < 0.4$).

The k_* parameters are given as pre-computed values which depend on the cut-off energy.

$$E\frac{dn_e}{dE} = a_0 \frac{E}{(E+a_1)(E+a_2)^s}$$

with:

$$a_0 = k_0 e^{(k_1 s + k_2 s^2)}$$

$$a_2 = 168.168 - 42.1368s$$

$$a_1 = 6.42522 - 1.53183s$$

Electron Energy Distribution: Comparison

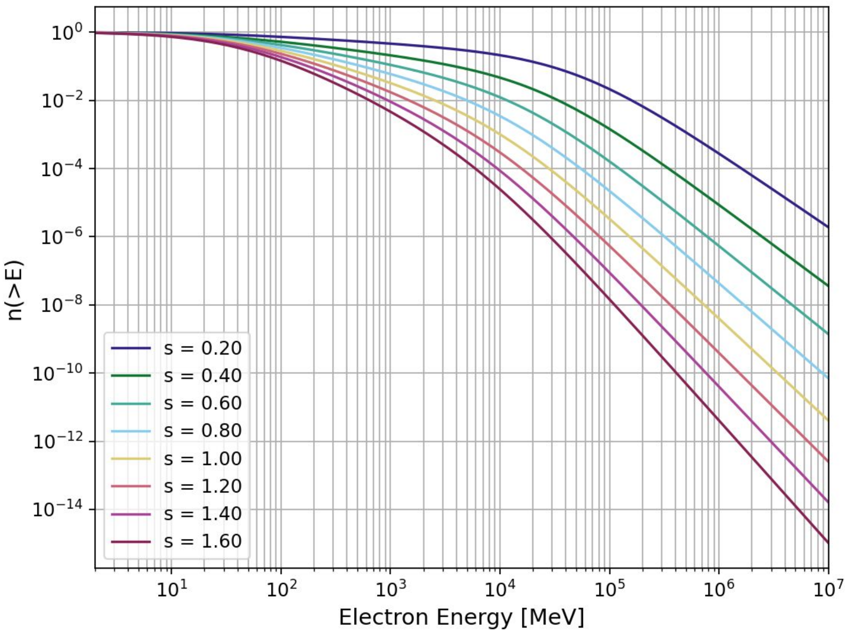

Hillas

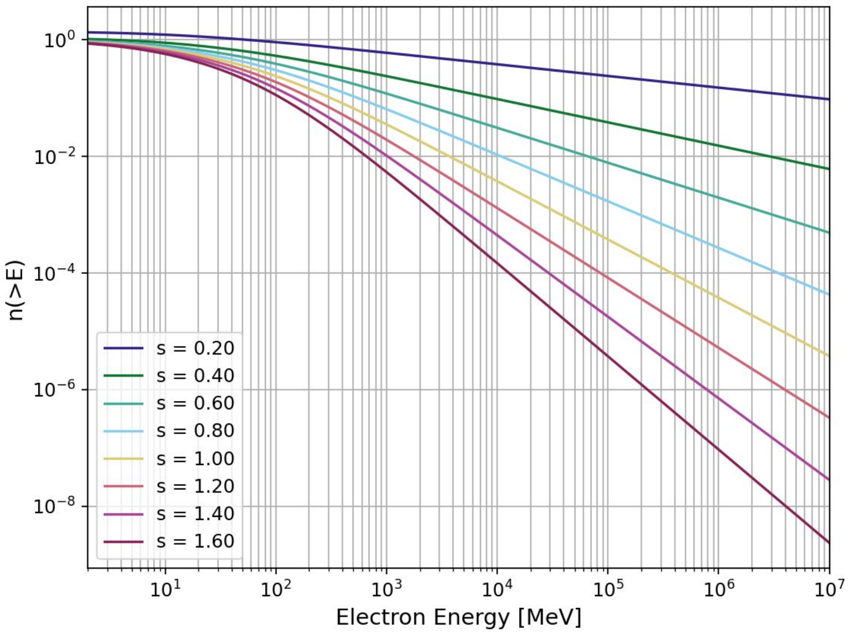

Nerling

Electron Energy Distribution: Comparison

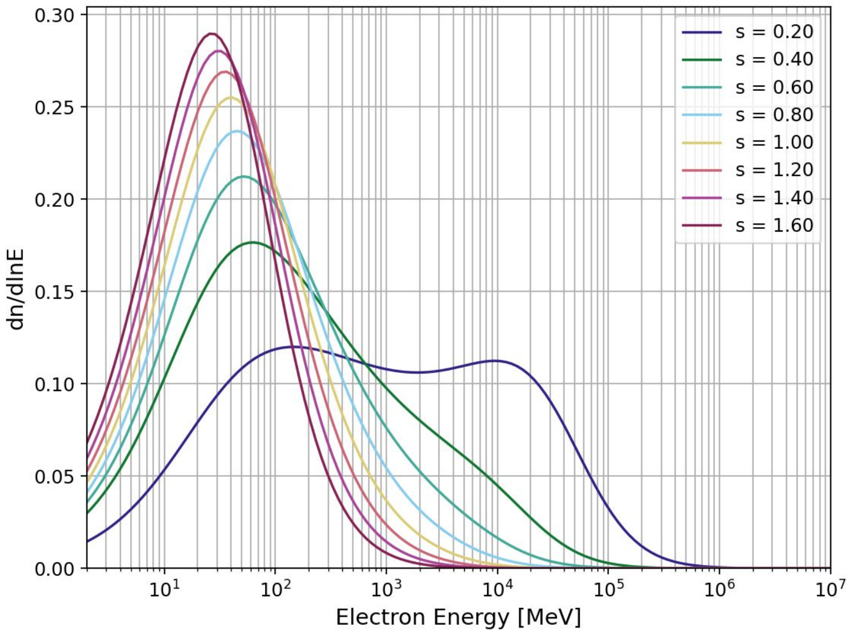

Hillas

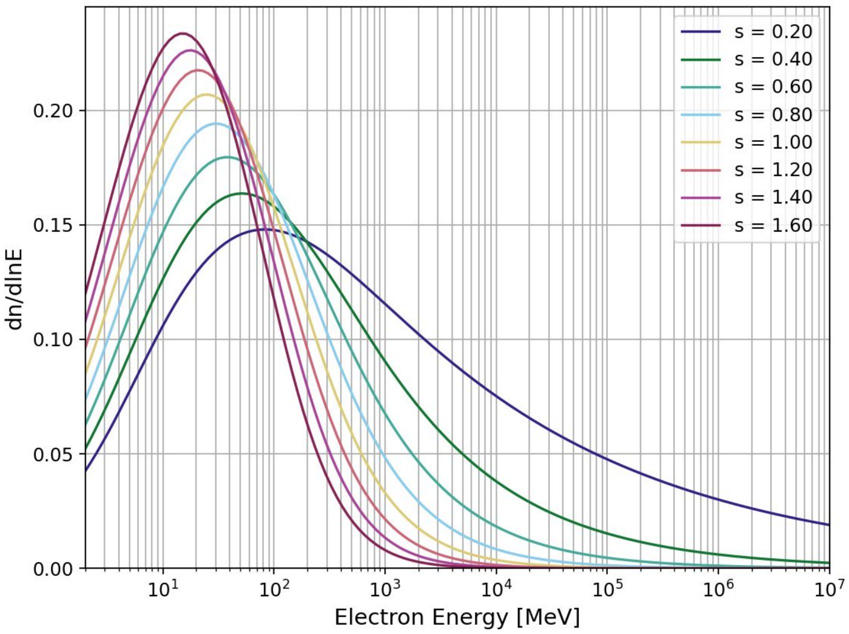

Nerling

14

Longitudinal Template

$$\frac{dN_\gamma^{(EAS)}}{d\epsilon} = \int_{X_{min}}^{X_{max}} \frac{dX}{\rho(X)\,c}\, Tr(\epsilon, \Delta X) \boxed{N(X)} \int_{E_{min}}^{E_{max}} dE\, \frac{dn_e}{dE}(E, s(X))\, \frac{dN_\gamma^{(1)}}{d\epsilon}(E, \epsilon)$$

Longitudinal template

The shower size as a function of grammage is taken from CORSIKA simulation results with:

- a 100 PeV proton primary,
- QGSJETII-04 hadronic interaction model for high-energies,
- GHEISHA 2002d hadronic model for low-energies,
- slant depth, curved atmosphere, and upward geometry options enabled.

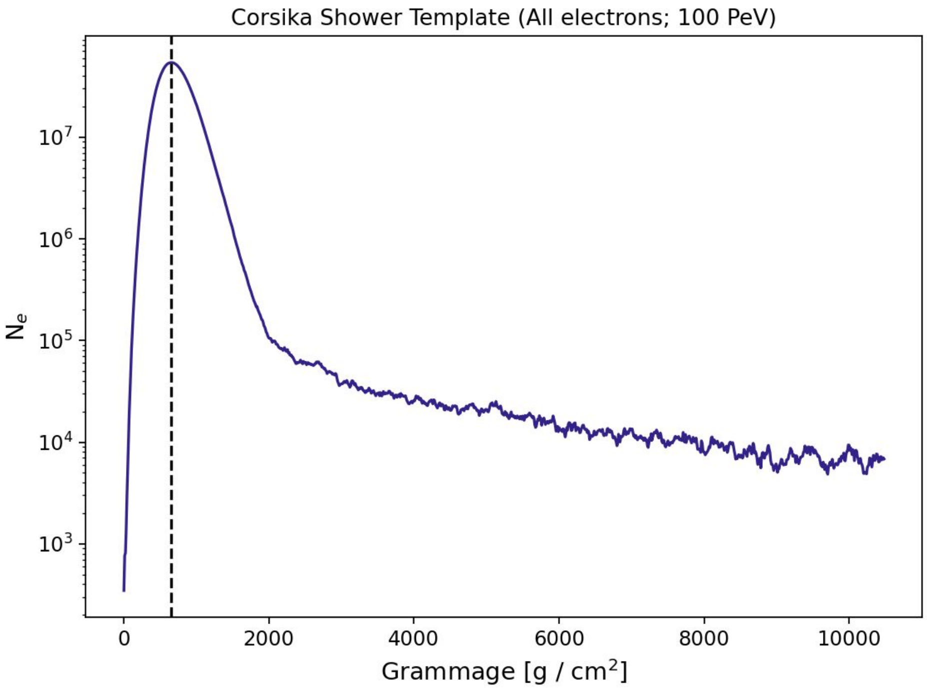

16

Longitudinal template

- This CORSIKA template is the same as the 'default' template used by EASCherSim for the Cherenkov photon fluxes.
- An interpolator is used to evaluate the shower size at arbitrary grammage values.
- Other templates may be used for the computation with relative ease.

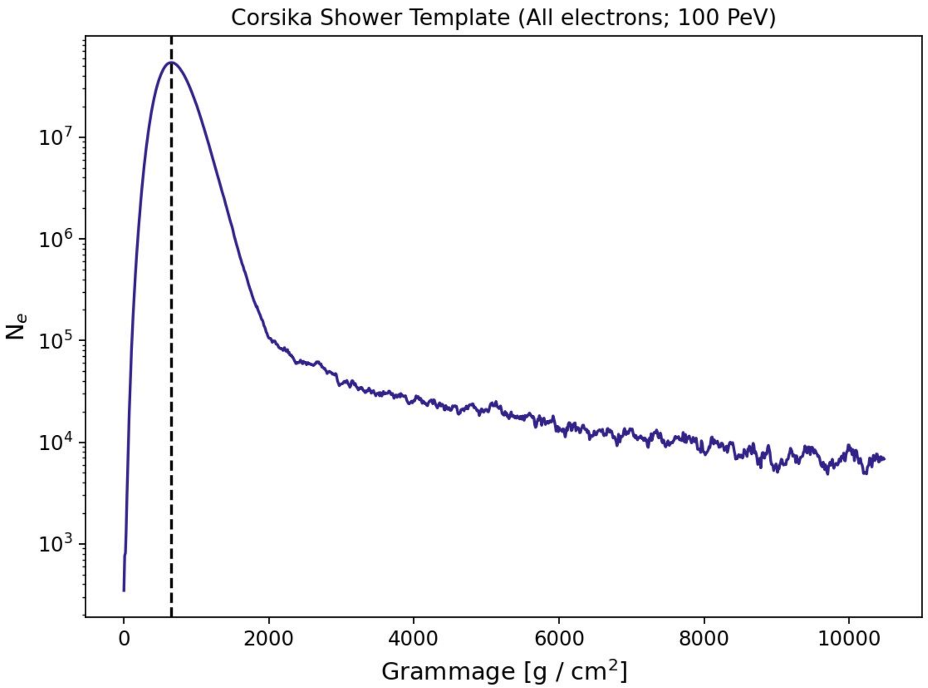

Atmosphere

$$\frac{dN_\gamma^{(EAS)}}{d\epsilon} = \int_{X_{min}}^{X_{max}} \boxed{\frac{dX}{\rho(X)\, c}}\, Tr(\epsilon, \Delta X)\, N(X) \int_{E_{min}}^{E_{max}} dE\, \frac{dn_e}{dE}(E, s(X))\, \frac{dN_\gamma^{(1)}}{d\epsilon}(E, \epsilon)$$

Atmosphere: Density

$$\rho(z) = \begin{cases} \frac{b}{c} e^{-z/c} & \text{if } z \leq 100 \text{ km} \\ \frac{b}{c} & \text{if } z > 100 \text{ km} \end{cases}$$

$z(\mathrm{km})$	$b(\mathrm{g/cm^2})$	$c(\mathrm{cm})$
0-4	1222.6562	994186.38
4-10	1144.9069	878153.55
10-40	1305.5948	636143.04
40-100	540.1778	772170.16
100-112	1	1×10^9

- The atmospheric density profile is based on the 1976 US Standard Atmosphere.
- Is is a multi-layer exponential model (above) with parameters depending on the atmosphere layer (right).
- Consistent with the models used both by CORSIKA to generate the shower size template, and by EASCherSim.

Atmosphere: Density Plot

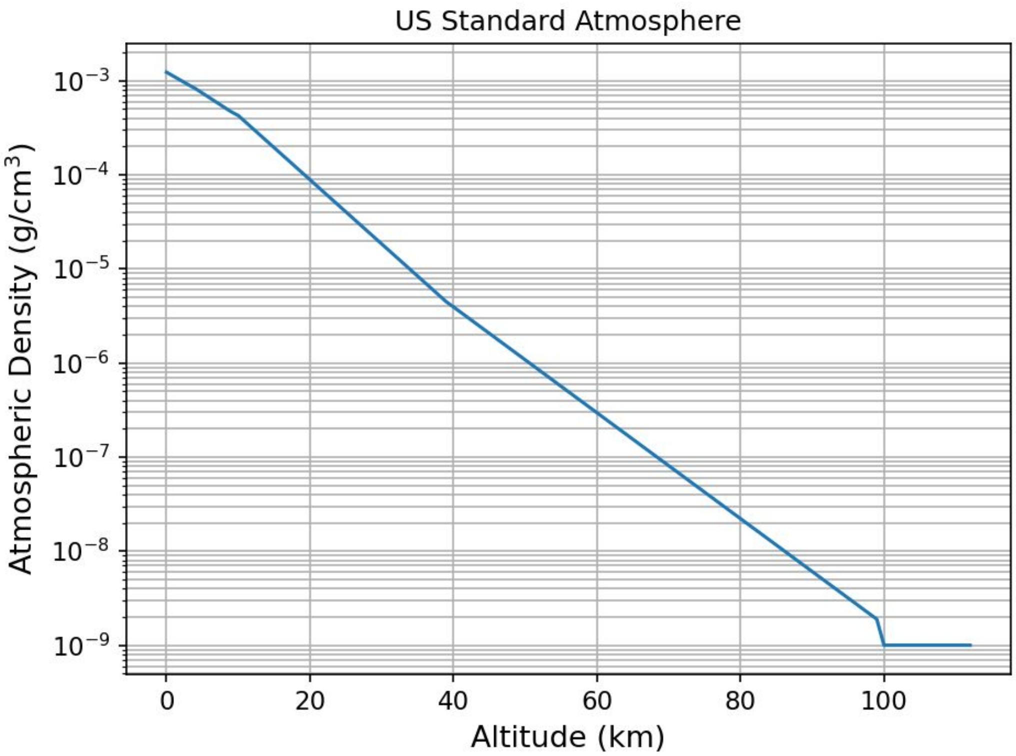

Integration Over Grammage (Geometry)

$$\frac{dN_\gamma^{(EAS)}}{d\epsilon} = \boxed{\int_{X_{min}}^{X_{max}} \frac{dX}{\rho(X)\, c}} Tr(\epsilon, \Delta X)\, N(X) \int_{E_{min}}^{E_{max}} dE\, \frac{dn_e}{dE}(E, s(X))\, \frac{dN_\gamma^{(1)}}{d\epsilon}(E, \epsilon)$$

Integration Over Grammage: Geometry

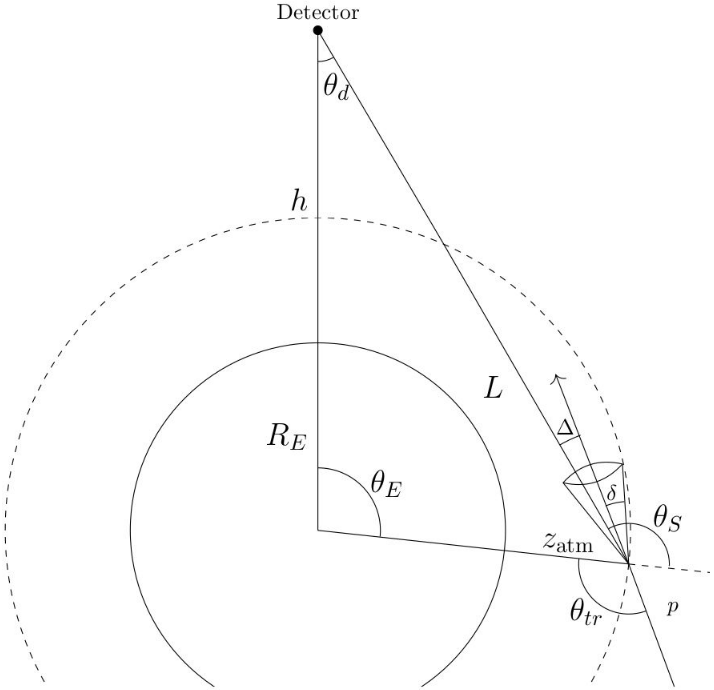

Above-the-limb events

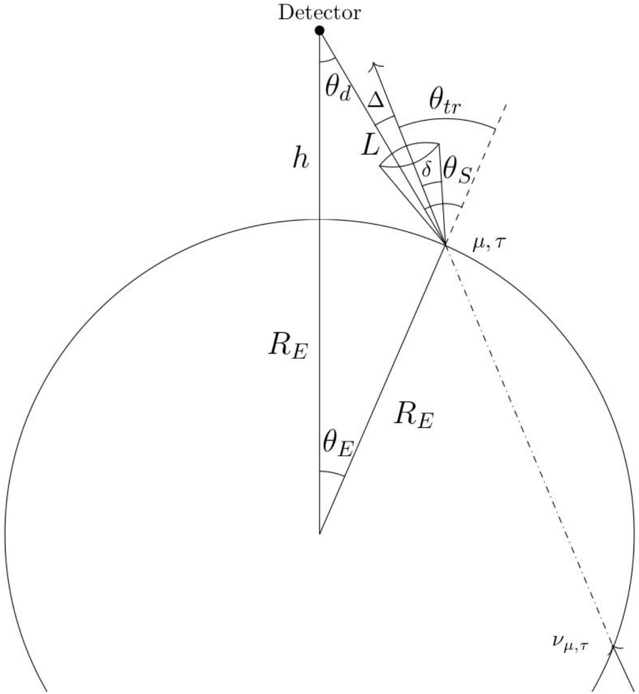

Below-the-limb events

Atmospheric Attenuation

$$\frac{dN_\gamma^{(EAS)}}{d\epsilon} = \int_{X_{min}}^{X_{max}} \frac{dX}{\rho(X)\,c} \boxed{Tr(\epsilon, \Delta X)} N(X) \int_{E_{min}}^{E_{max}} dE\, \frac{dn_e}{dE}(E, s(X))\, \frac{dN_\gamma^{(1)}}{d\epsilon}(E, \epsilon)$$

Atmospheric Attenuation

- Photons interact with the atmosphere along their path to the detector.
- The probability of survival depends on the integral along the line of sight of an attenuation coefficient.
- For a single element, this attenuation coefficient is inversely proportional to the interaction cross section.

$$\mathrm{Tr}(\epsilon) = \exp\left[-\int_0^L \mu_a(\epsilon)\,\rho(l)\,dl\right]$$

with:

$$\mu_X(\epsilon)^{-1} = \frac{M(X)}{N_A}\,\sigma_X(\epsilon)$$

Atmospheric Attenuation

Since:

- the atmospheric density as a function of the altitude is known, and
- the altitude profile of a particle along the line of sight is known from the geometry,

the transmission factor may be written as a function of the grammage between the point of emission and the detector position.

$$\mathrm{Tr}(\epsilon) = \exp\left[-\int_0^L \mu_a(\epsilon)\, \rho(l)\, dl\right]$$

$$\Big\downarrow \; dX = \rho\, dl$$

$$\mathrm{Tr}(\epsilon, \Delta X) = \exp\left[-\int_{X_i}^{X_f} \mu_a(\epsilon)\, dX\right]$$

$$\mathrm{Tr}(\epsilon, \Delta X) = \exp\left[-\mu_a(\epsilon)\, \Delta X\right]$$

Atmospheric Attenuation: NIST XCOM

The NIST XCOM database was queried to obtained the attenuation coefficients:

- the 1976 US Standard Atmosphere composition (right) was used as the mixture composition for the query.
- the total attenuation coefficient is a weighted sum (by mass fraction) of the constituents' coefficients.
- mass fractions were computed from the volume fractions assuming ideal gas behavior.

Component	Volume Fraction	M ($gmol^{-1}$)
N_2	0.78084	28.0134
O_2	0.209476	31.9988
Ar	0.00934	39.948
CO_2	0.000314	44.0095
Ne	0.00001818	20.1797
He	0.00000524	4.0026
Kr	0.00000114	83.798
Xe	0.000000087	131.293
CH_4	0.000002	16.043
H_2	0.0000005	2.0159

Atmospheric Attenuation: Plots

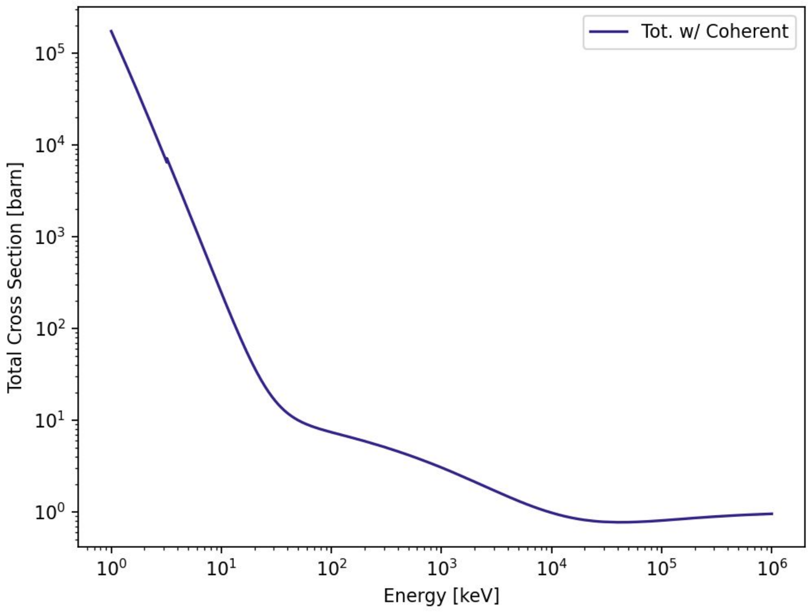

Effective Cross Section

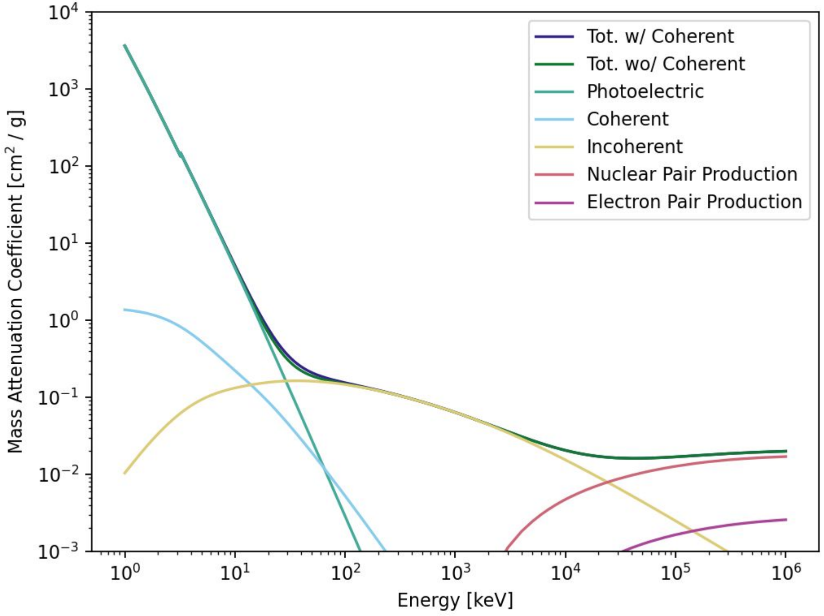

Mass Attenuation Coefficient

Transmission Factors ([10 keV, 30 keV] band)

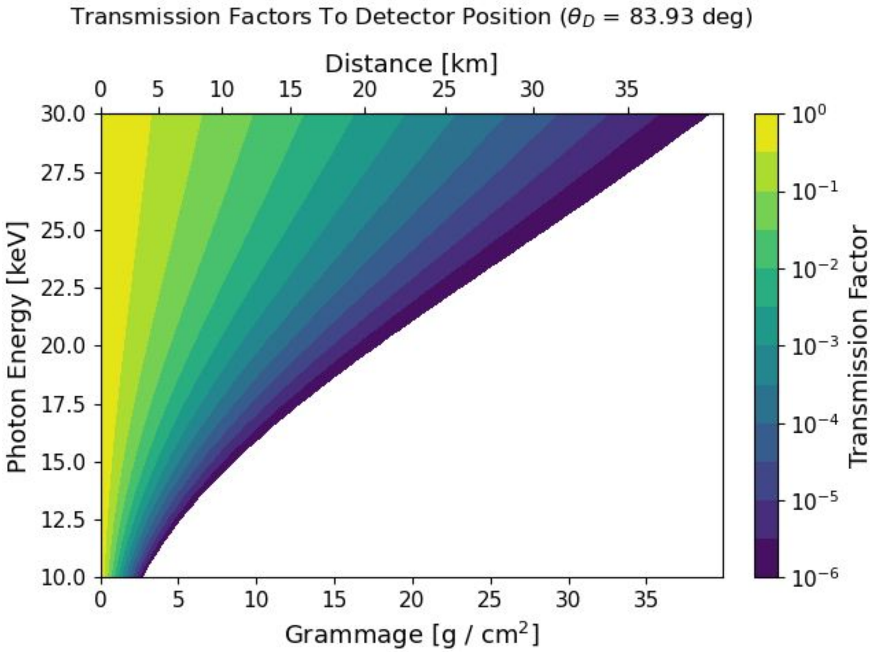

Limb-viewing

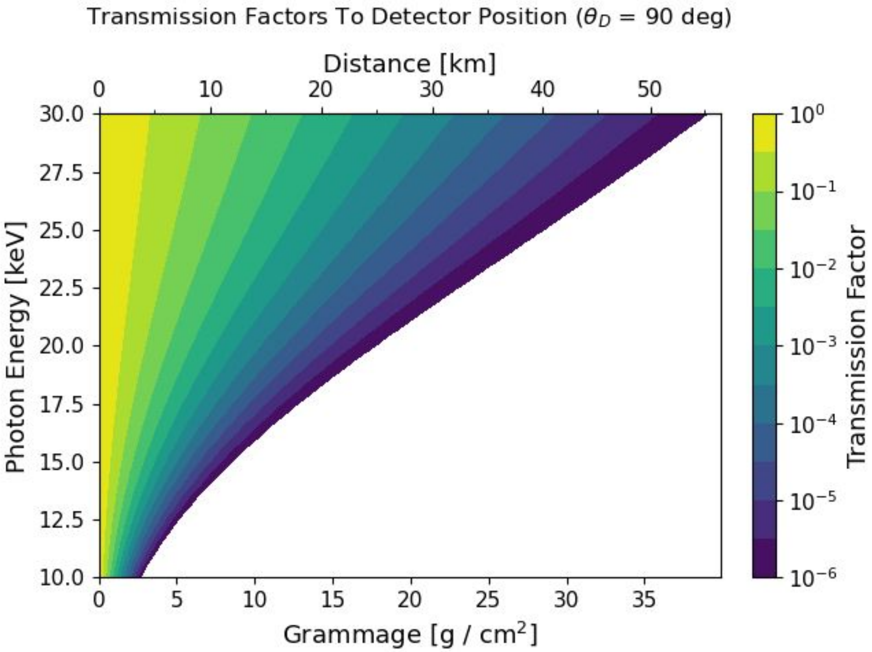

Horizontal-viewing

Transmission Factors ([30 keV, 300 keV] band)

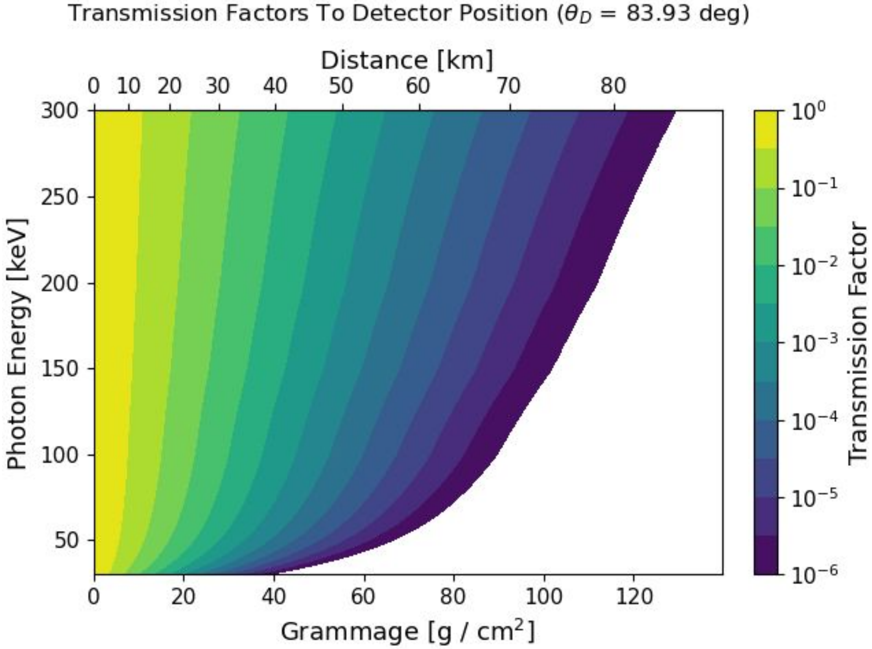

Limb-viewing

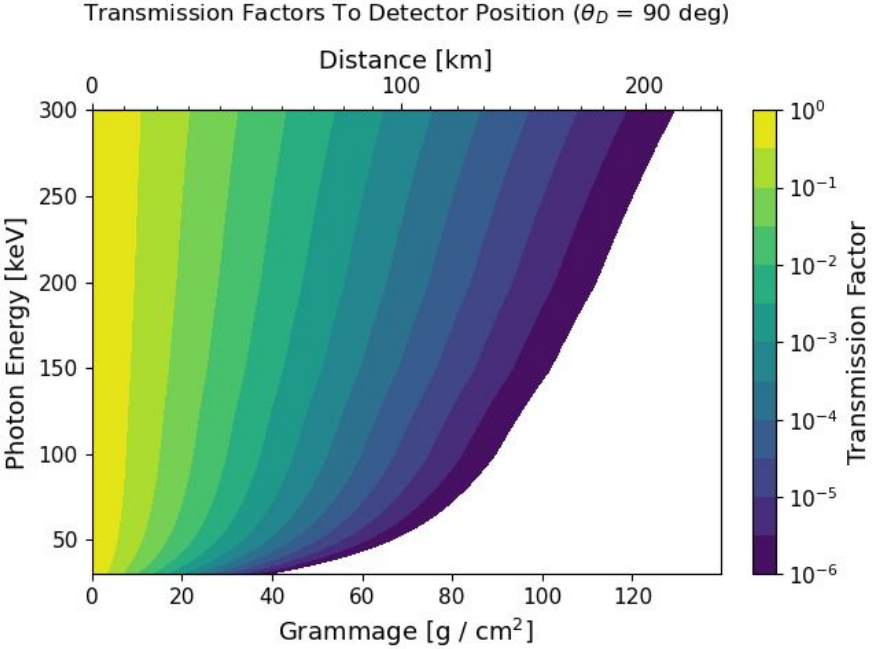

Horizontal-viewing

Transmission Factors ([100 keV, 4 MeV] band)

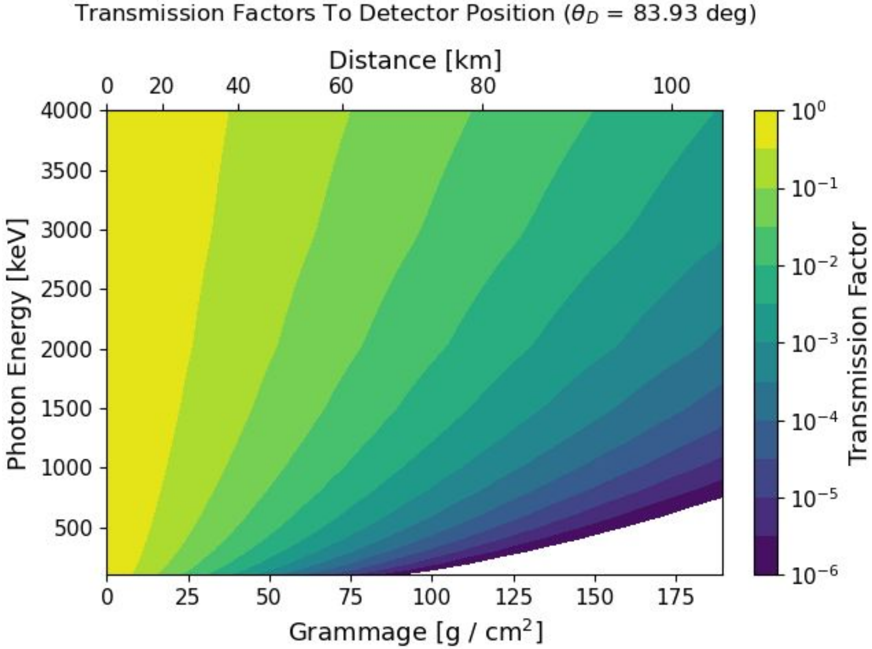

Limb-viewing

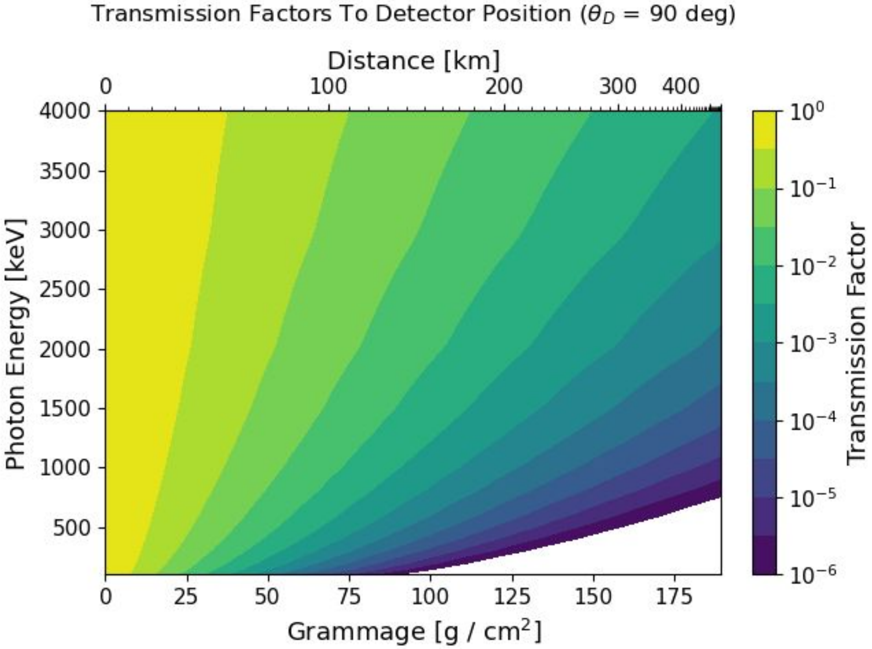

Horizontal-viewing

30

Number of Detected Photons

$$\boxed{\frac{dN_\gamma^{(EAS)}}{d\epsilon}} = \int_{X_{min}}^{X_{max}} \frac{dX}{\rho(X)\,c}\, Tr(\epsilon, \Delta X)\, N(X) \int_{E_{min}}^{E_{max}} dE\, \frac{dn_e}{dE}(E, s(X))\, \frac{dN_\gamma^{(1)}}{d\epsilon}(E, \epsilon)$$

Number of Detected Photons: The Recipe

For a given particle trajectory, characterized by its **viewing angle**, the number of photons reaching and ideal detection plane is estimated as follows:

- The initial interaction grammage is determined by the geometry and primary type:
  - For protons, X_0 is fixed at 30 g/cm^2.
  - For tau leptons, the grammage is computed as the column density from the Earth's surface to the point where the tau lepton decays – which is fixed at 5 km (average decay length at 100 PeV).
- The primary energy is set to at 100 PeV for proton showers, while for tau showers it is halved to account for the fraction of energy lost to the outgoing neutrino.

Number of Detected Photons: The Recipe

The number of photons per unit photon energy, both emitted and transmitted through the atmosphere, is computed by **numerically integrating** the **master formula** over a **grid**.

- γ energy: logarithmic binning from 10 keV to 10 MeV, with 25 samples per decade.
- e^- energy: logarithmic binning from 100 GeV to 1 PeV, with 100 samples per decade.
- Grammage: linear binning w/ 10 samples per unit grammage, starting at the first interaction point and extending to the detection plane.

After computing the photon emission spectra, the number of expected photons within the PBR instrumental energy bands, is determined by integrating these spectra.

A scan over viewing angles from 0° to 100° (in 1° increments) is performed, first using the Hillas parameterization, and then repeated with the Nerling parameterization.

Number of Detected Photons: The Results

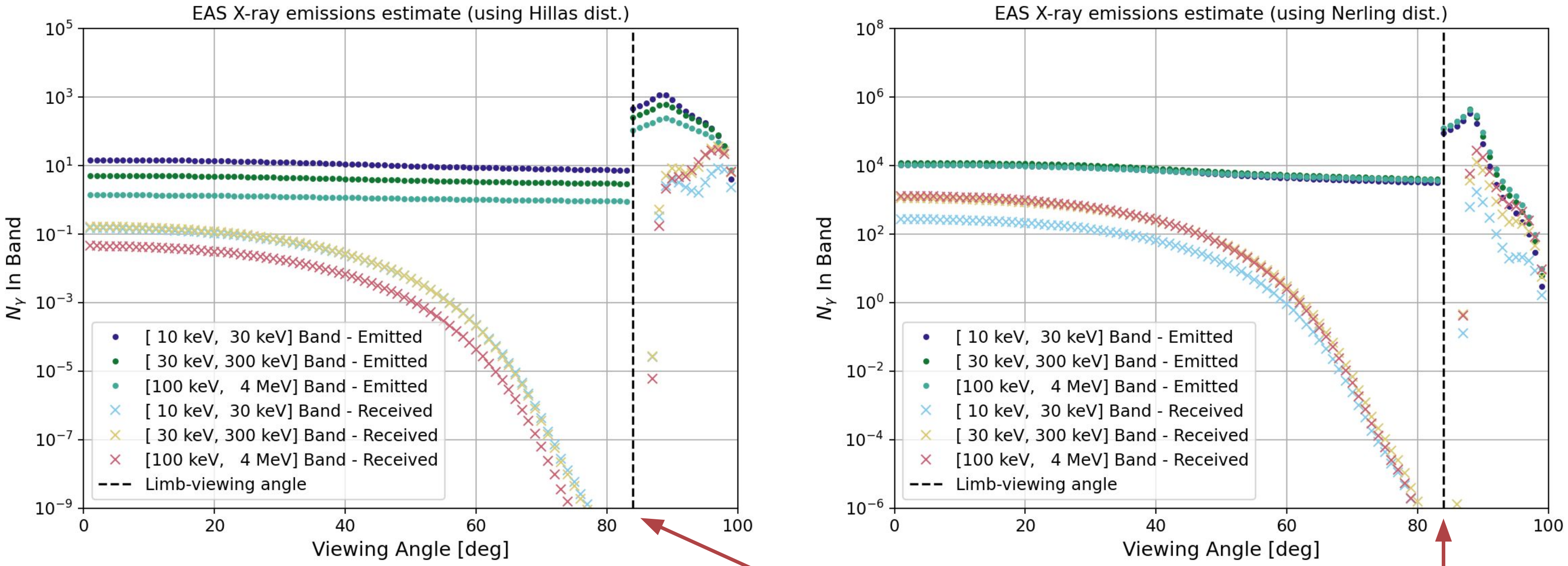

With Hillas Dist.

Limb-viewing angle for PBR

With Nerling Dist.

Conclusions

The **results**:

- the number of emitted photons reaching the detection plane depends critically on the electron energy distribution assumed for the computation.
- for HAHAs, using the Nerling dist.: ~10^2 to 10^4 γ's reach the detection plane.
- for HAHAs, using the Hillas dist.: only ~10 γ's reach the detection plane.
- overall, for below-the-limb trajectories, less photons arrive to the detection plane since the shower develops in a denser layer of the atmosphere.

Currently under discussion:

- The appropriate angular distributions and lateral distributions to use for high-energy e^- (E > 100 GeV) in very young showers ($0.1 < s < 0.5$).
- The effect of the magnetic field on the γ's spatial distribution on the plane.

Plots

Using the Nerling distribution

Above-the-limb Spectra (Nerling)

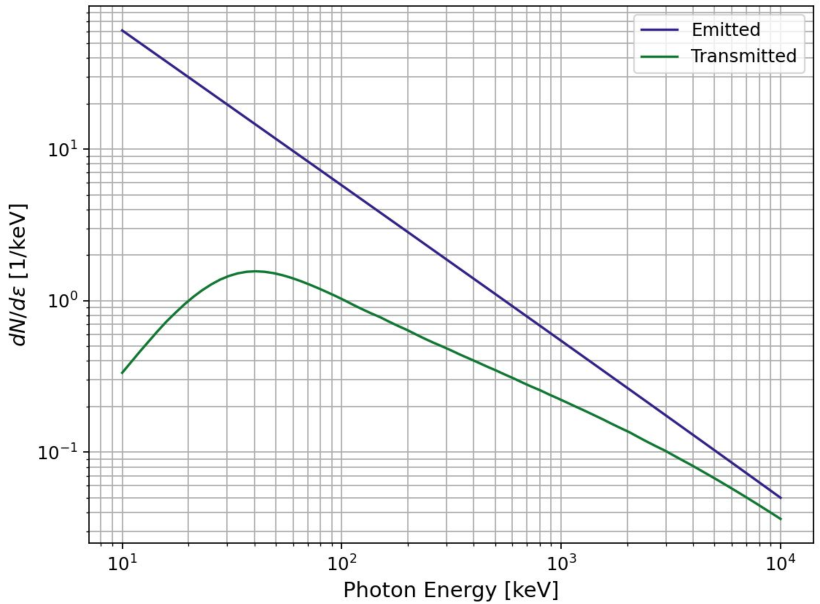

94.00° viewing (Nadir) angle

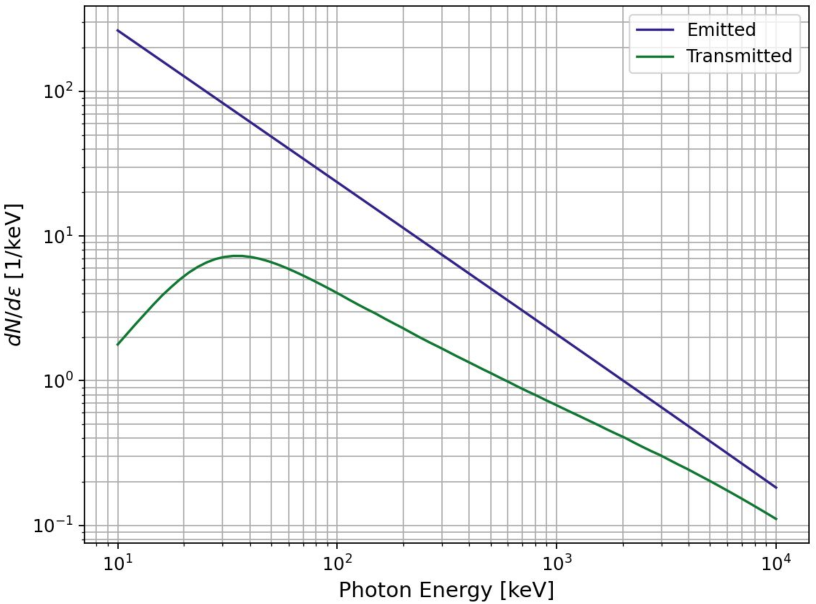

92.00° viewing (Nadir) angle

Above-the-limb Spectra (Nerling)

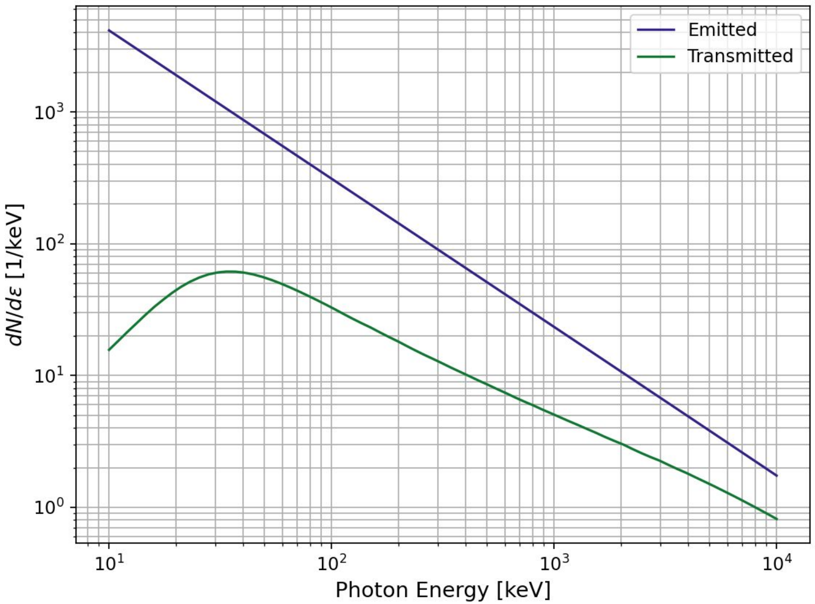

90.00° viewing (Nadir) angle

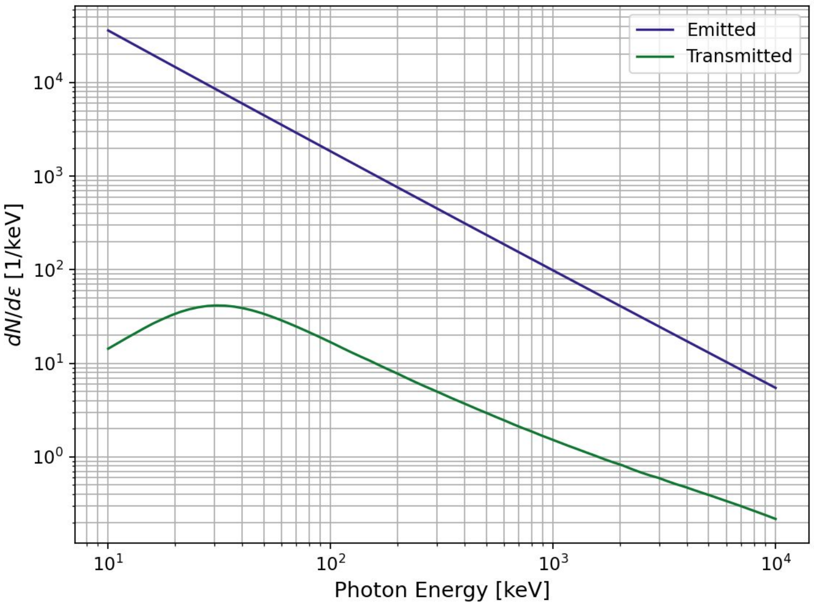

88.00° viewing (Nadir) angle

Above-the-limb Spectra (Nerling)

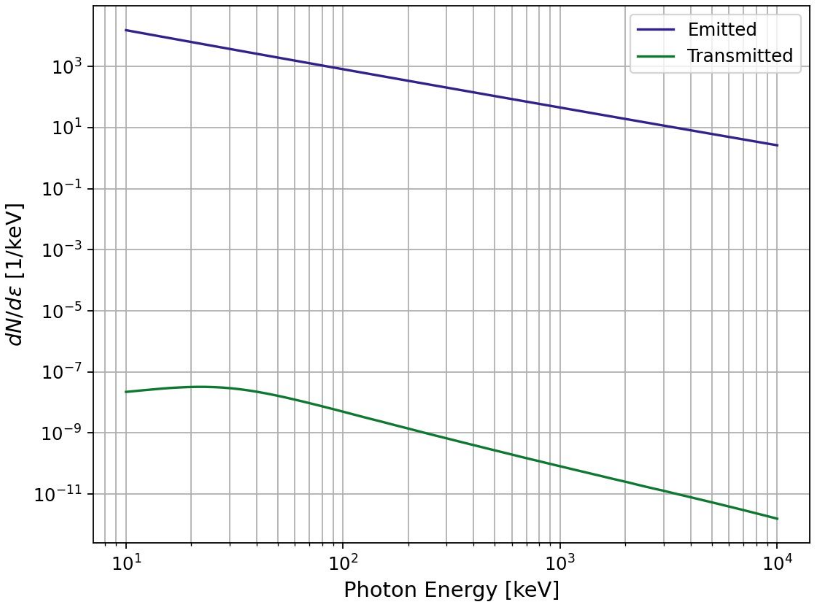

86.00° viewing (Nadir) angle

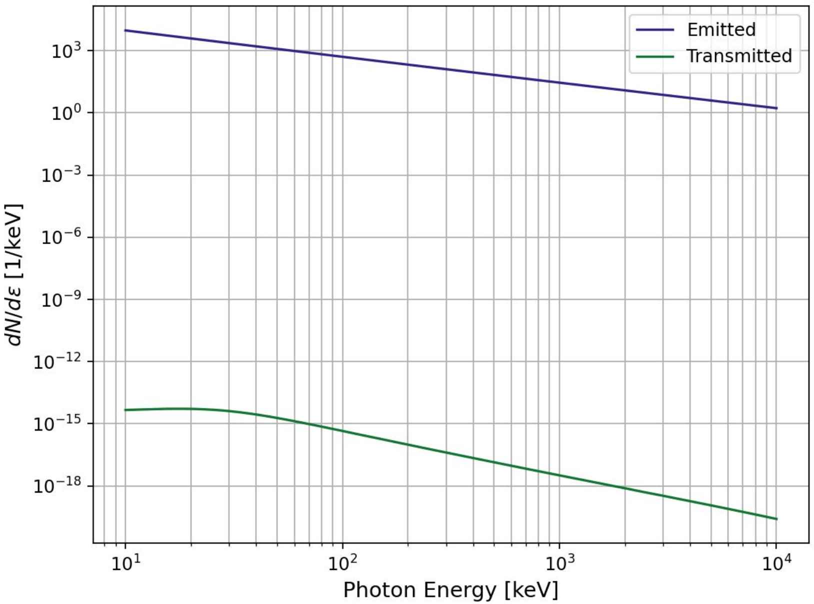

84.00° viewing (Nadir) angle

Below-the-limb Spectra (Nerling)

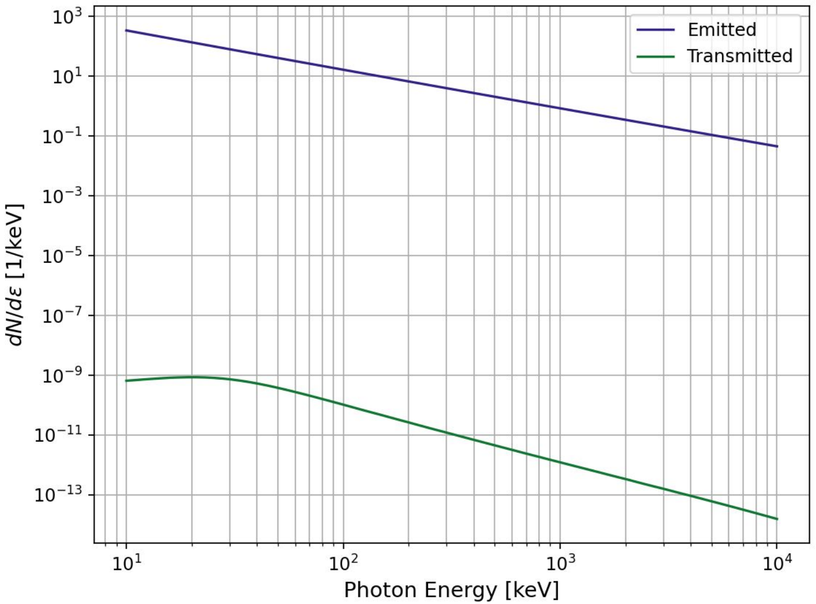

83.00° viewing (Nadir) angle
3.49° emergence angle

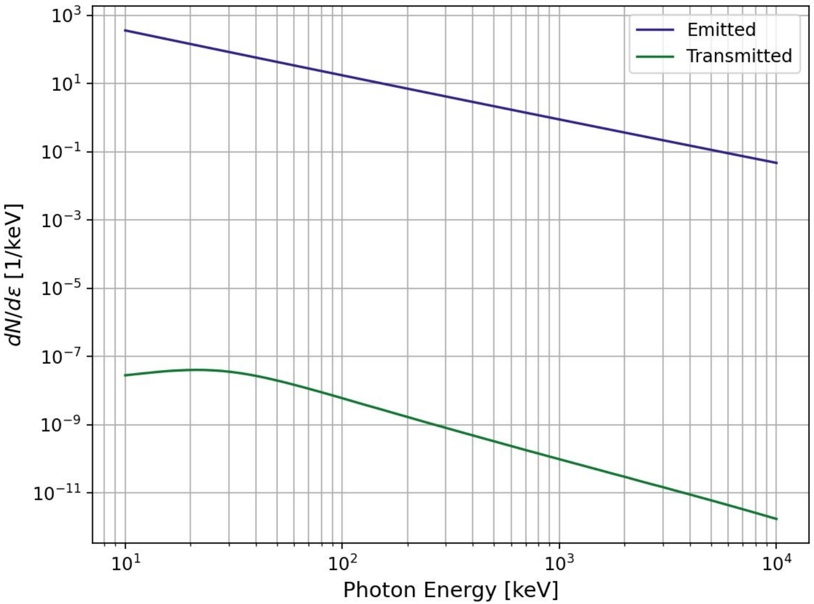

80.00° viewing (Nadir) angle
7.96° emergence angle

Below-the-limb Spectra (Nerling)

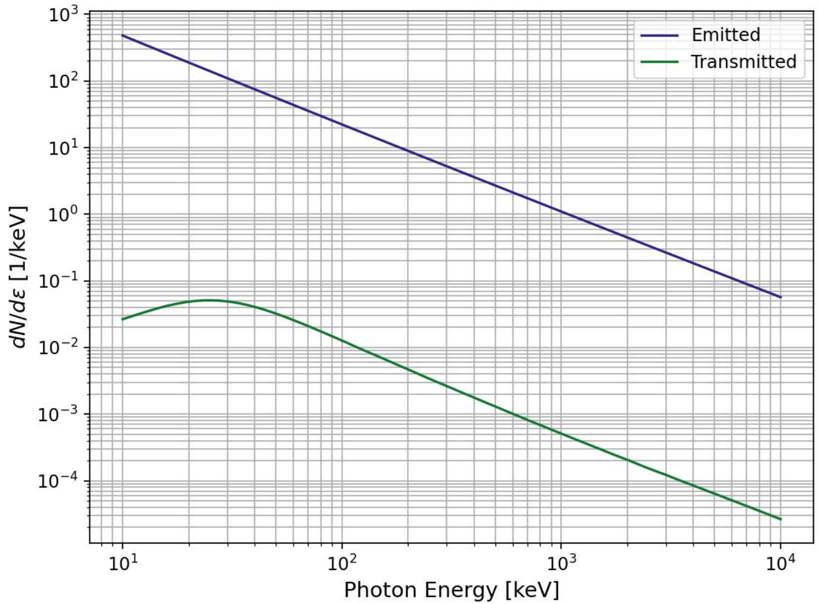

60.00° viewing (Nadir) angle
29.44° emergence angle

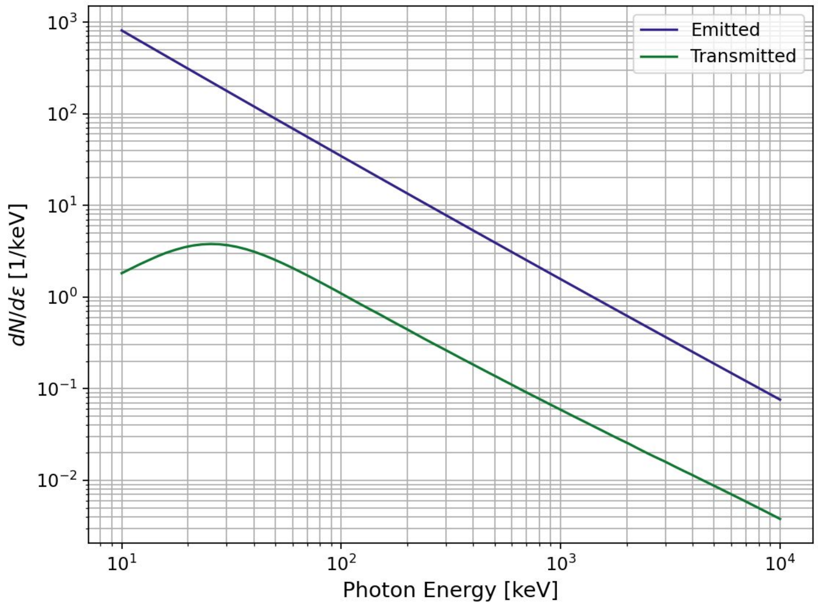

40.00° viewing (Nadir) angle
49.73° emergence angle

Below-the-limb Spectra (Nerling)

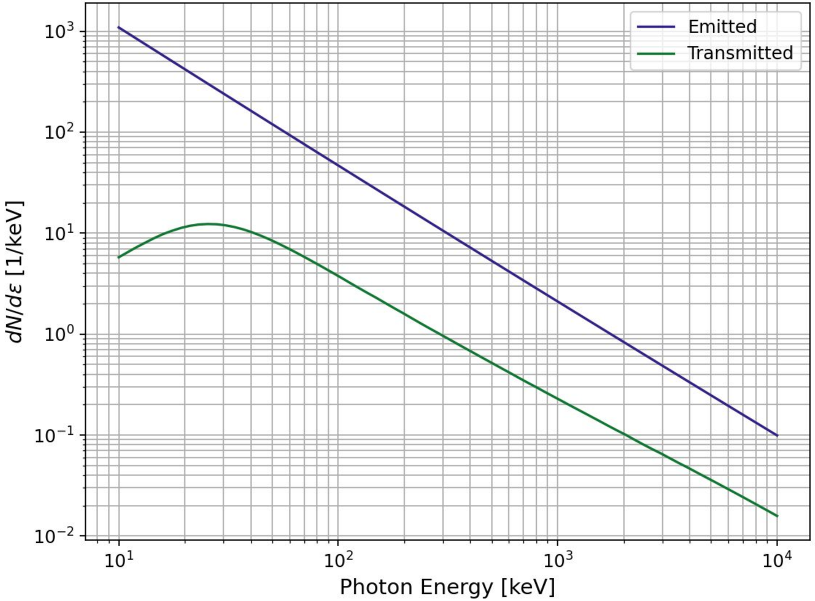

20.00° viewing (Nadir) angle
69.88° emergence angle

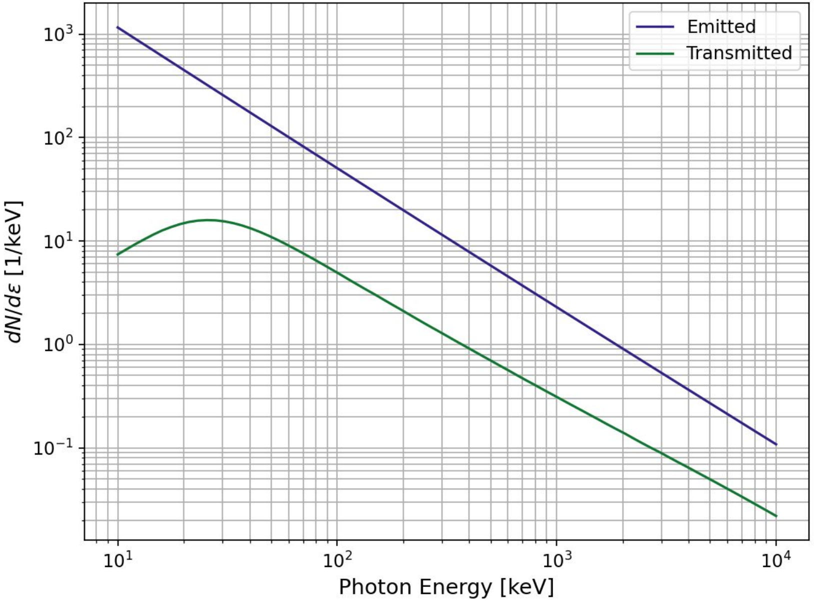

0.00° viewing (Nadir) angle
90.00° emergence angle

Photon emissions as a function of distance between emission- and detection-point

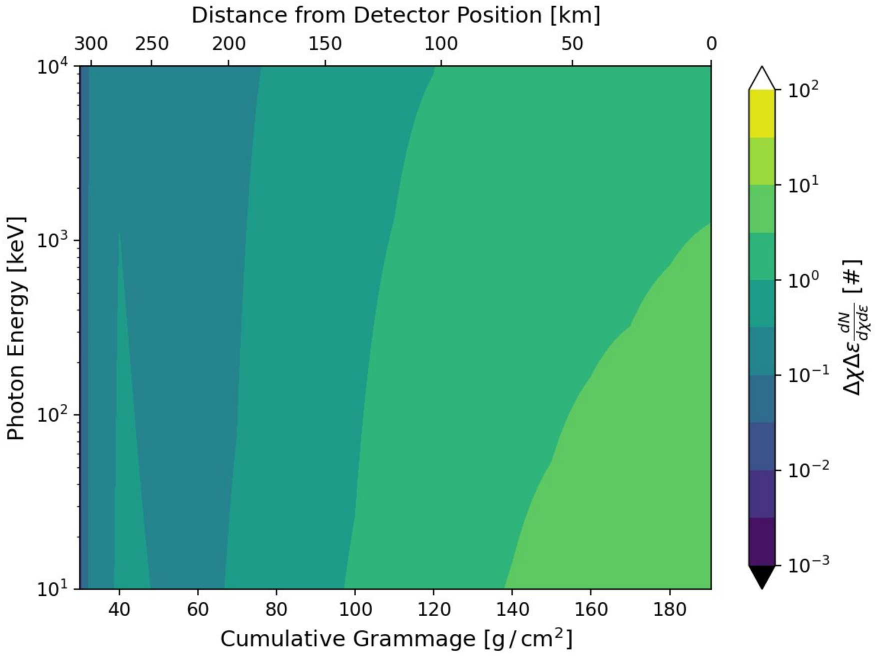

90.00° viewing (Nadir) angle
Emitted

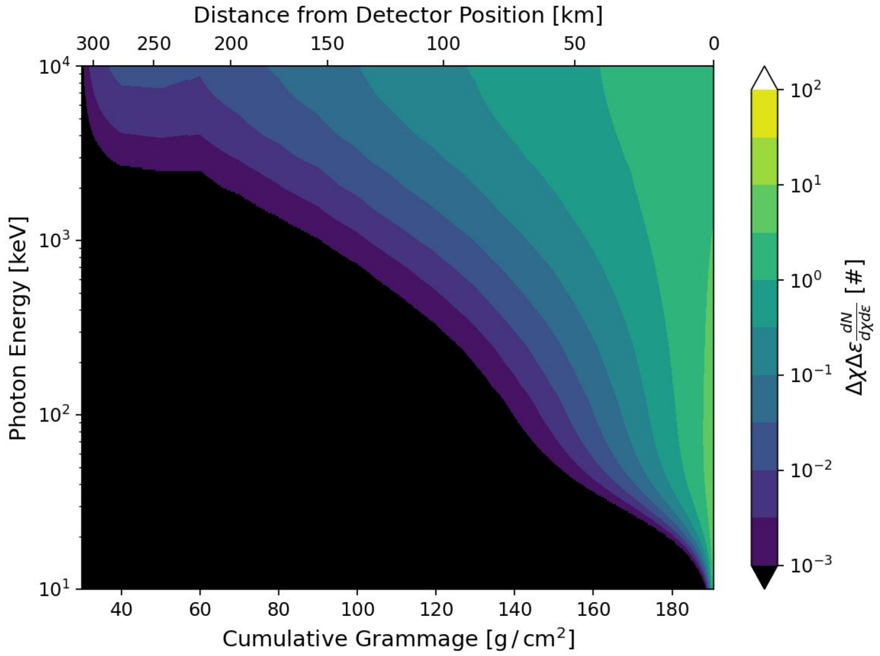

90.00° viewing (Nadir) angle
Transmitted

Photon emissions as a function of distance between emission- and detection-point

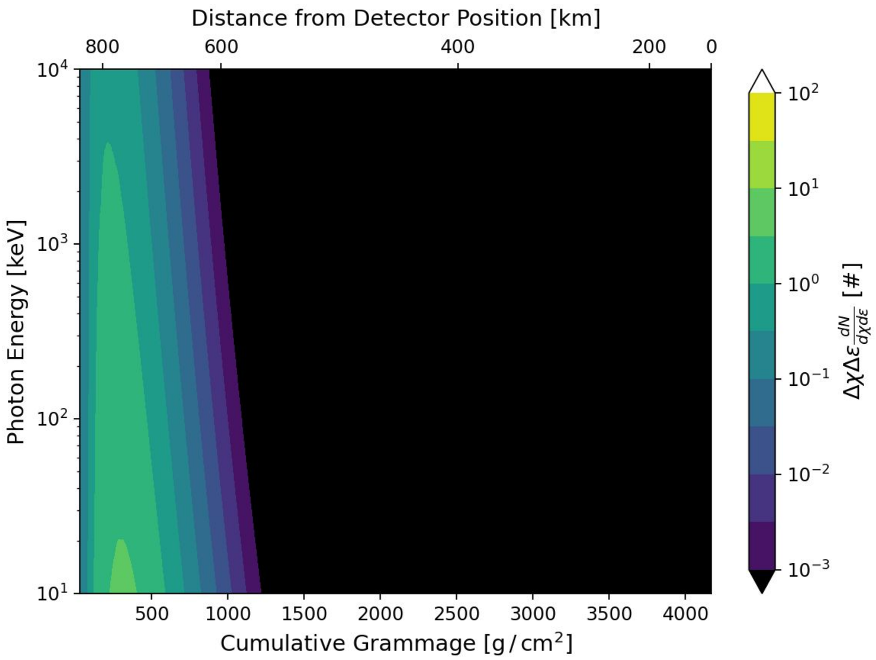

86.00° viewing (Nadir) angle
Emitted

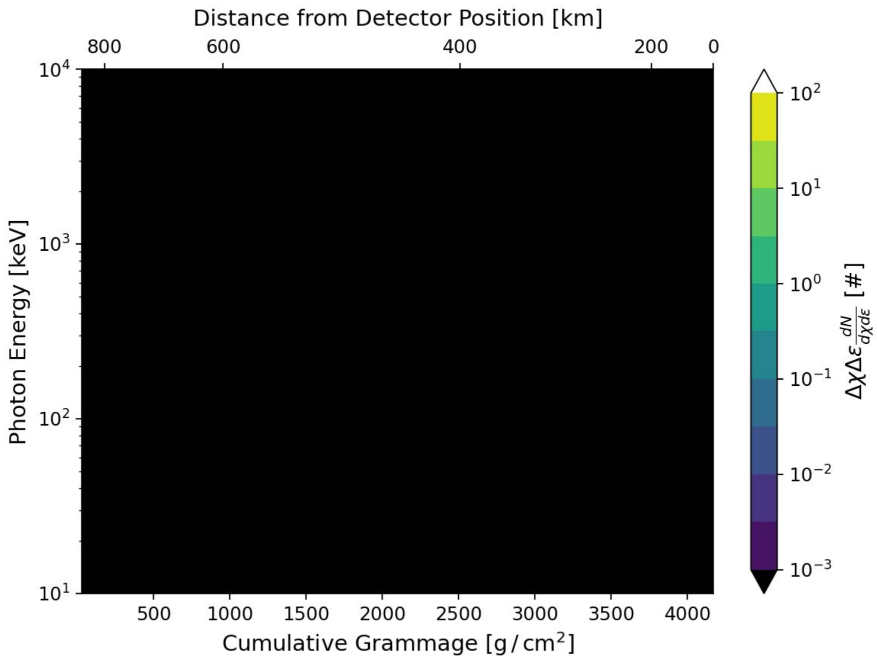

86.00° viewing (Nadir) angle
Transmitted

Photon emissions as a function of distance between emission- and detection-point

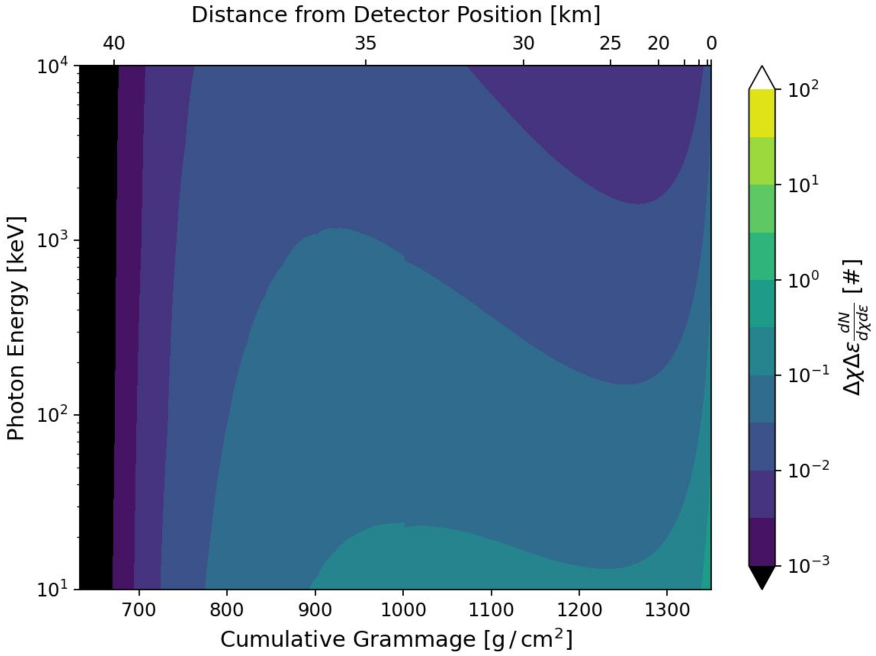

40.00° viewing (Nadir) angle
Emitted

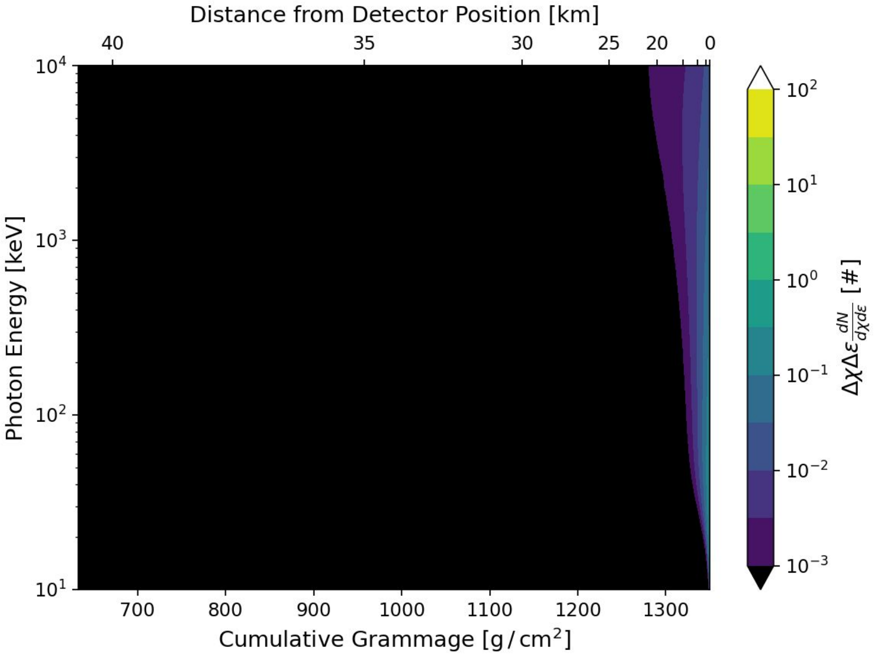

40.00° viewing (Nadir) angle
Transmitted

Photon emissions as a function of distance between emission- and detection-point

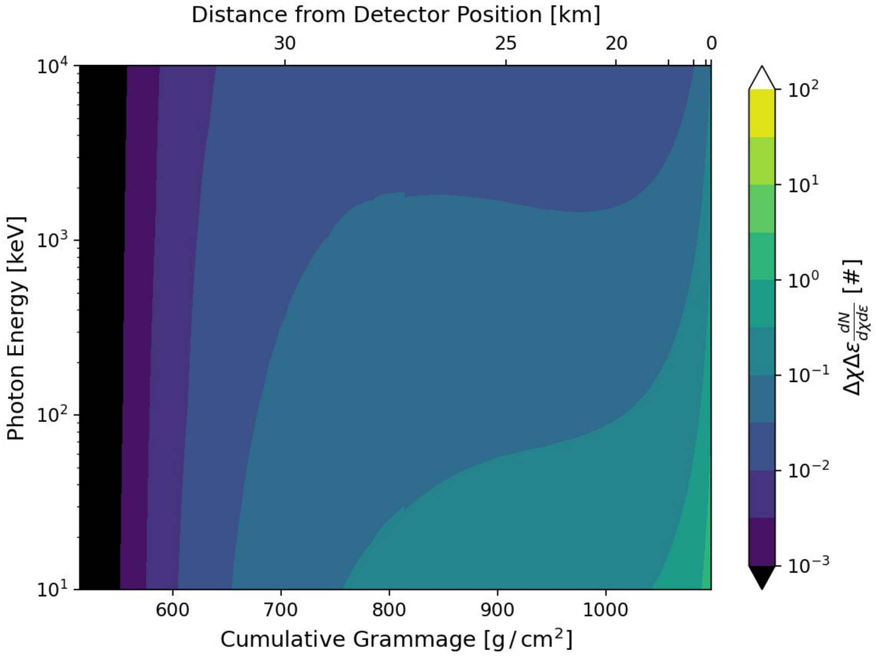

20.00° viewing (Nadir) angle
Emitted

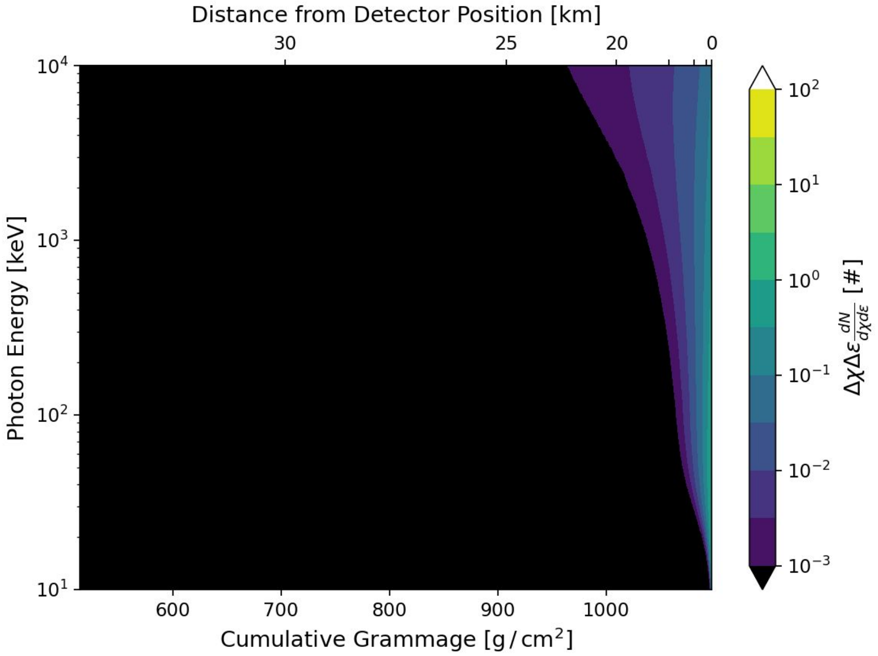

20.00° viewing (Nadir) angle
Transmitted

Photon emissions as a function of distance between emission- and detection-point

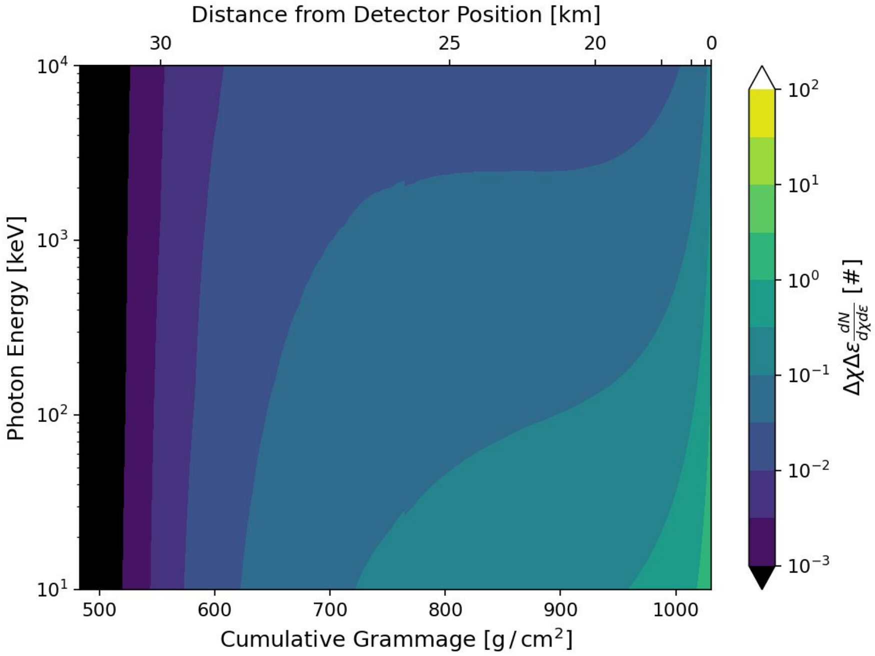

0.00° viewing (Nadir) angle
Emitted

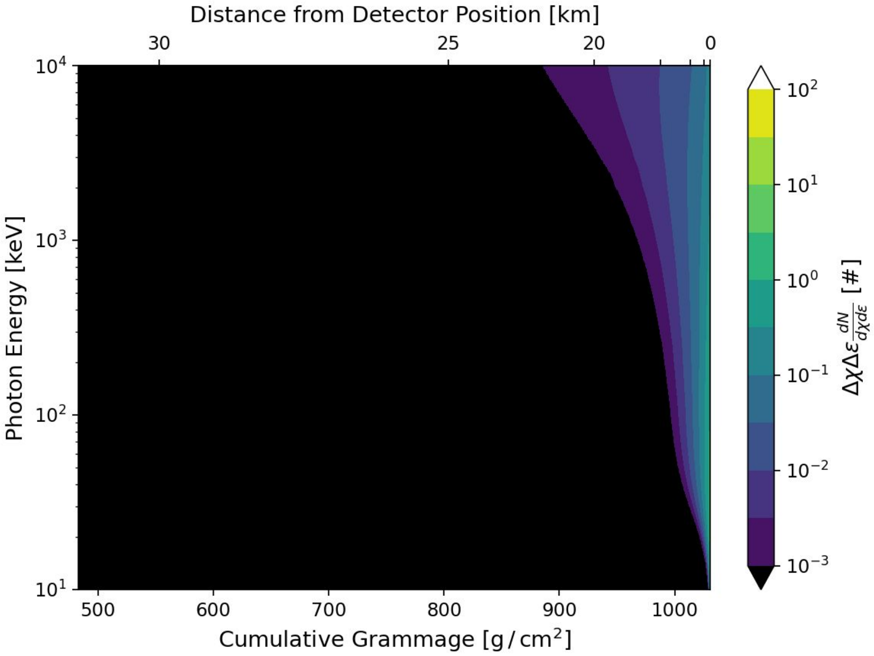

0.00° viewing (Nadir) angle
Transmitted

Using the Hillas distribution

Above-the-limb Spectra (Hillas)

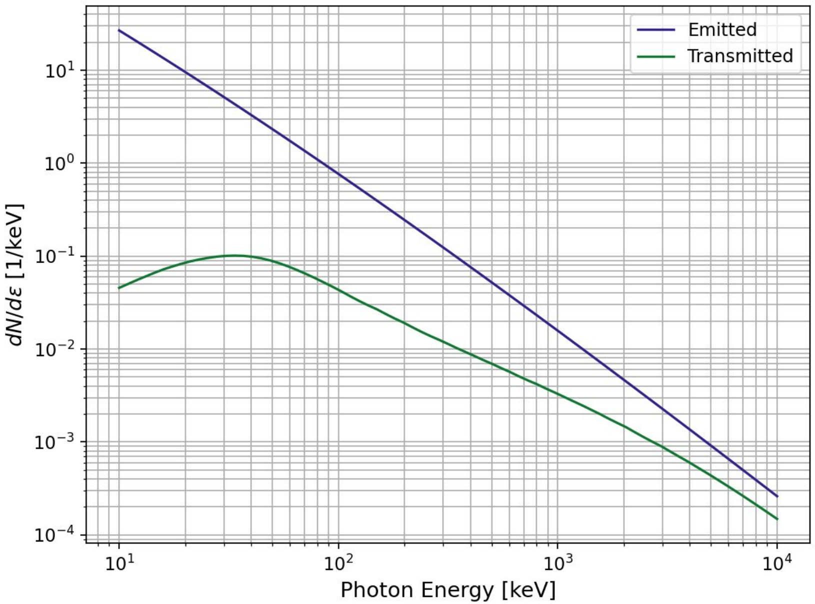

94.00° viewing (Nadir) angle

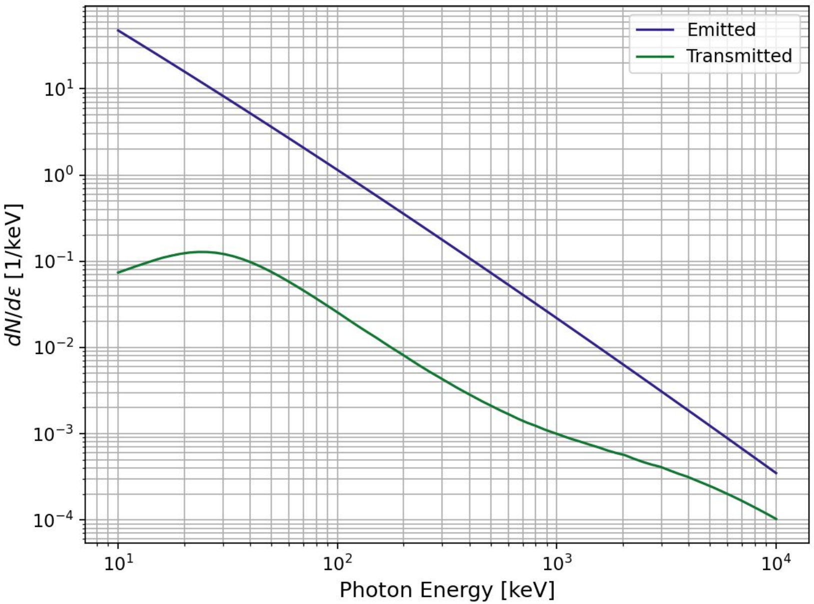

92.00° viewing (Nadir) angle

Above-the-limb Spectra (Hillas)

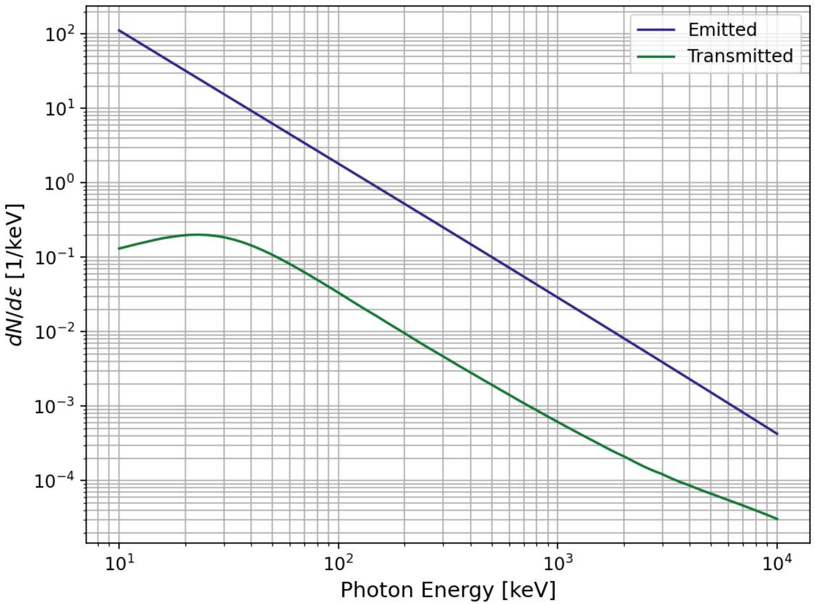

90.00° viewing (Nadir) angle

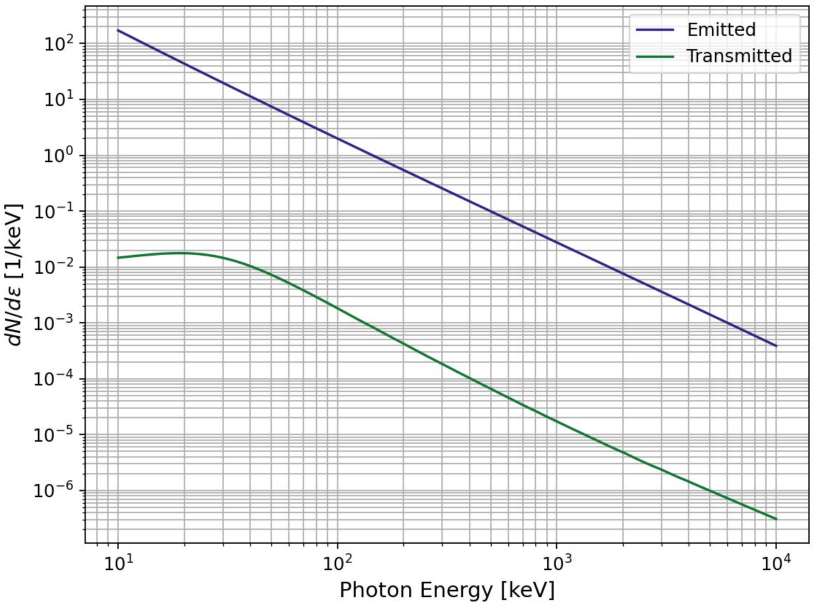

88.00° viewing (Nadir) angle

Above-the-limb Spectra (Hillas)

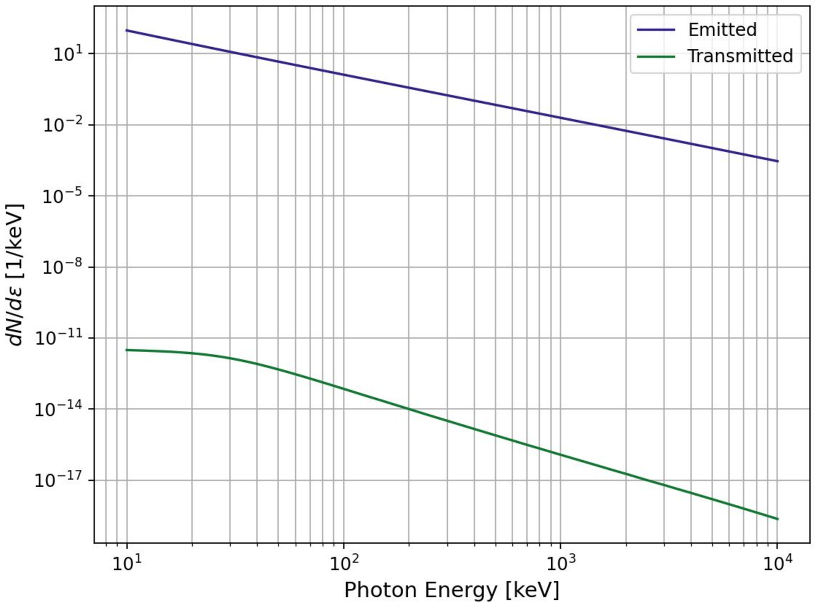

86.00° viewing (Nadir) angle

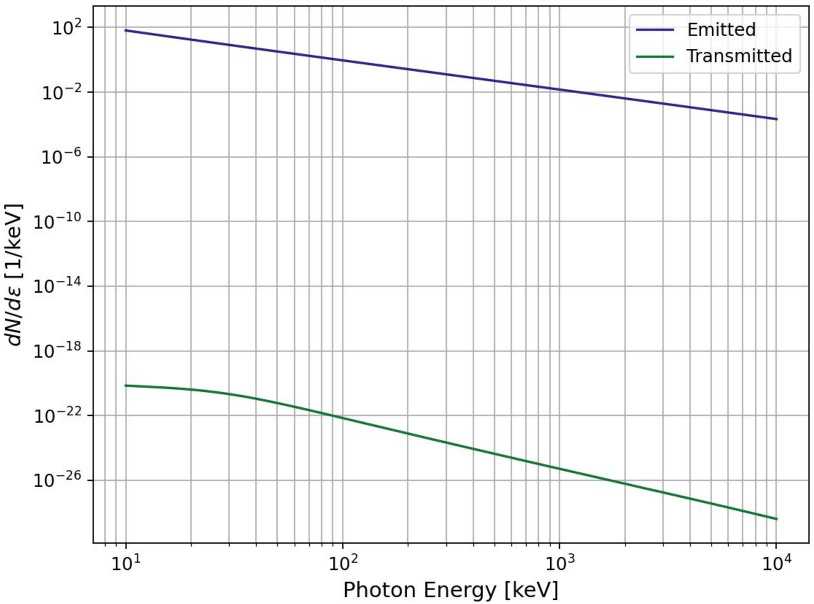

84.00° viewing (Nadir) angle

Below-the-limb Spectra (Hillas)

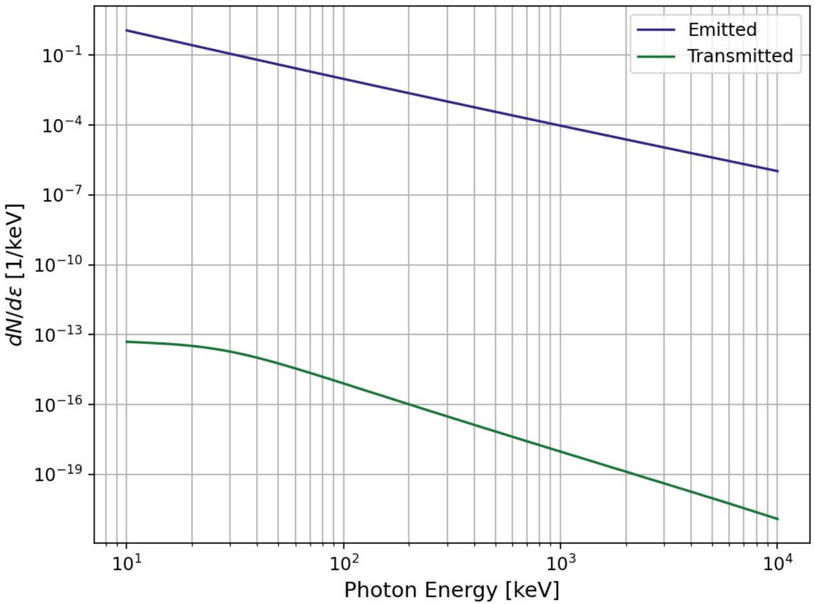

83.00° viewing (Nadir) angle
3.49° emergence angle

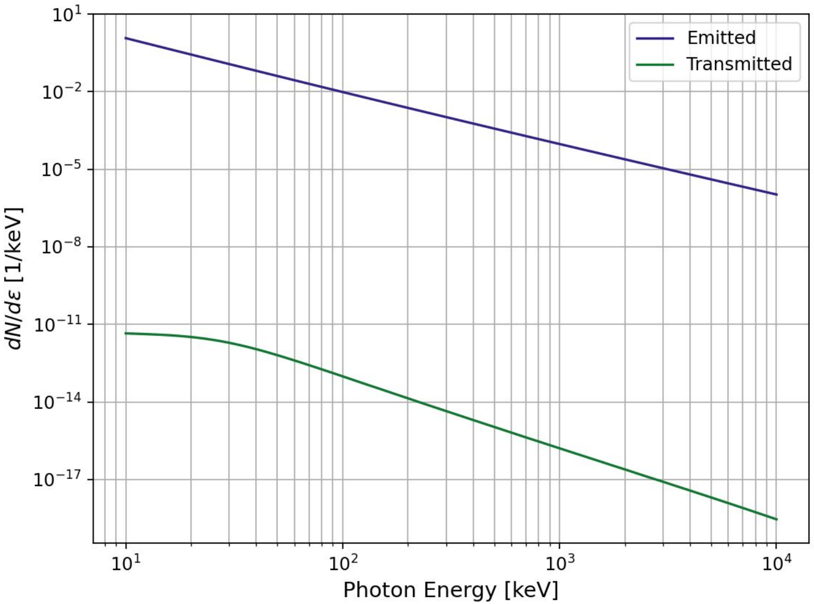

80.00° viewing (Nadir) angle
7.96° emergence angle

Below-the-limb (Hillas)

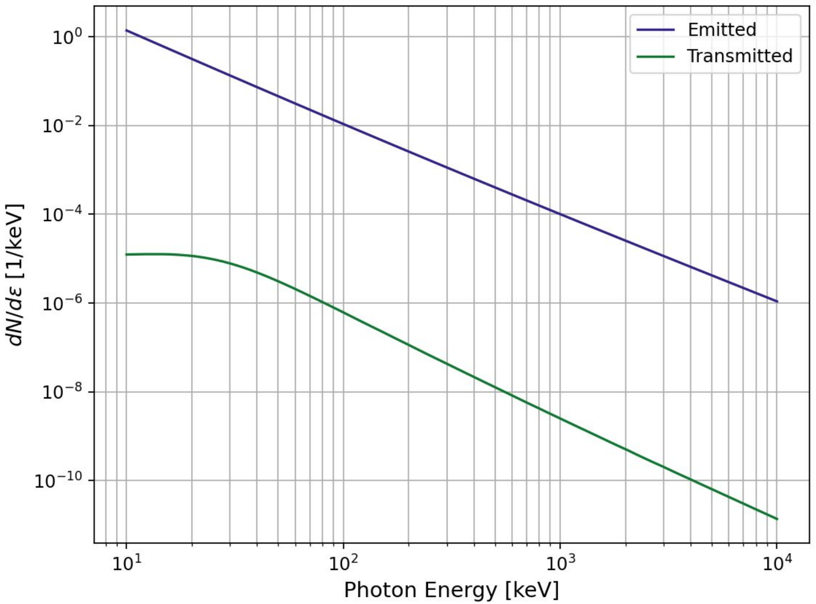

60.00° viewing (Nadir) angle
29.44° emergence angle

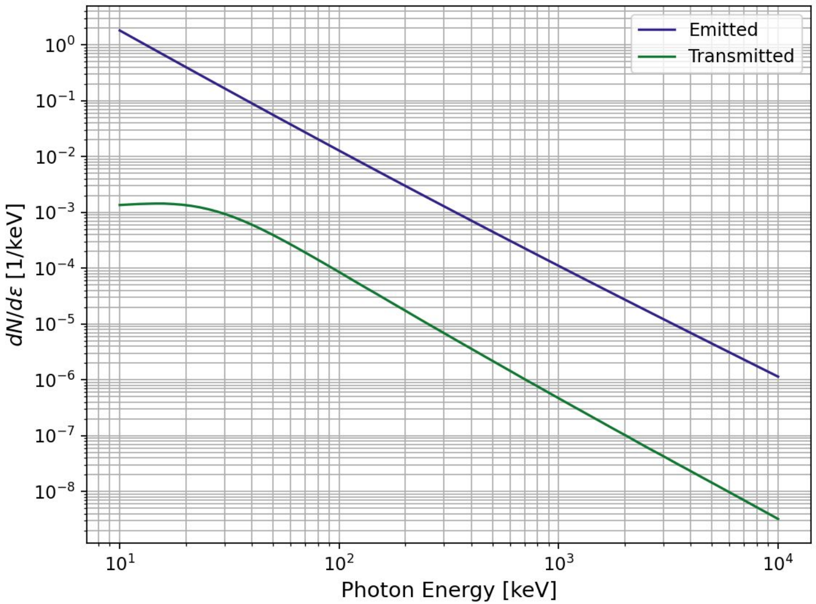

40.00° viewing (Nadir) angle
49.73° emergence angle

Below-the-limb (Hillas)

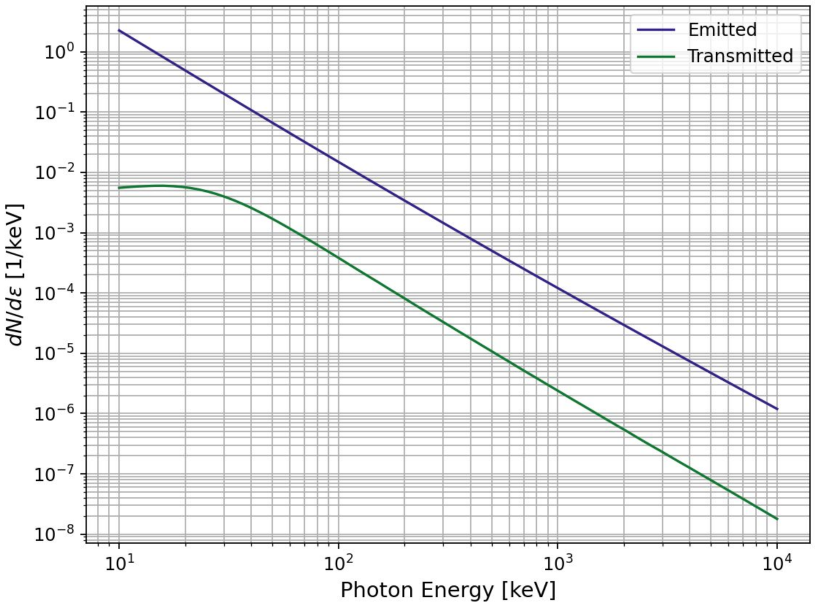

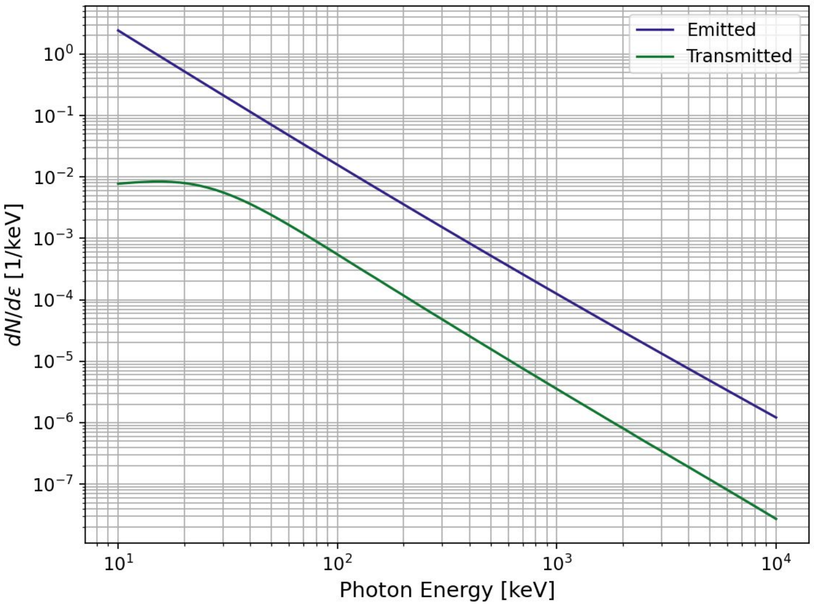

20.00° viewing (Nadir) angle
69.88° emergence angle

0.00° viewing (Nadir) angle
90.00° emergence angle